The T2K-ND280 upgrade proposal

P. Hamacher-Baumann, L. Koch, T. Radermacher, S. Roth, J. Steinmann

RWTH Aachen University, III. Physikalisches Institut, Aachen, Germany

V. Berardi, M.G. Catanesi, R.A. Intonti, L. Magaletti, E. Radicioni

INFN and Dipartimento Interateneo di Fisica, Bari, Italy

O. Beltramello, S. Bordoni, R. de Oliveira, A. De Roeck, R. Guida, D. Mladenov, M. Nessi, F. Pietropaolo, F. Resnati

CERN, Geneva, Switzerland

A. Marino, Y. Nagai, E. D. Zimmerman

University of Colorado at Boulder, Department of Physics, Boulder, Colorado, U.S.A.

C. Bronner, Y. Hayato, M. Ikeda, Y. Kataoka, M. Nakahata, Y. Nakajima, Y. Nishimura, H. Sekiya

University of Tokyo, Institute for Cosmic Ray Research, Kamioka Obs., Kamioka, Japan

S.Fedotov, M.Khabibullin, A.Khotjantsev, A.Kostin, Y.Kudenko, A.Mefodiev, O.Mineev, A.Smirnov, S.Suvorov, N.Yershov

Institute for Nuclear Research of the Russian Academy of Sciences, Moscow, Russia

J. Boix, M. Cavalli-Sforza, C. Jesus, M. Leyton, T. Lux, J. Mundet, F. Sanchez

Institut de Fisica d'Altes Energies (IFAE), The Barcelona Institute of Science and Technology, Bellaterra Spain

E. Atkin, P.J. Dunne, P. Jonsson, R.P. Litchfield, K.R. Long, W. Ma, T. Nonnenmacher, J. Pasternak, J. Pozimski, A. Sztuc, Y. Uchida, W. Shorrock, M.O. Wascko, C.V.C. Wret

Imperial College, London, United Kingdom

CERN-SPSC-2018-001 / SPSC-P-357
09/01/2018

M. Hartz, B. Quilain, M. Vagins

Kavli Institute for the Physics and Mathematics of the Universe (WPI), University of Tokyo, Kashiwa, Chiba, Japan

S. Aune, S. Bolognesi , D. Calvet, P. Colas, A. Delbart, S. Emery, M. Lamoureux, E. Mazzucato, G. Vasseur, M. Zito

IRFU, CEA Saclay, Gif-sur-Yvette, France

A. Blondel, A. Bravar, F. Cadoux, A. Korzenev, L. Maret, P. Mermod, L. Nicola, E. Noah, S. Parsa, D. Sgalaberna*

University of Geneva, Section de Physique, DPNC, Geneva, Switzerland

S.Cao, M.Friend, Y.Fujii, T.Hasegawa, T.Ishida, T.Kobayashi, T.Maruyama, T.Matsubara, T.Nakadaira, K.Nakayoshi, Y.Oyama, K.Sakashita, T.Sekiguchi, S.Y.Suzuki, M.Tada, T.Tsukamoto, Y.Yamada

High Energy Accelerator Research Organization (KEK) and JPARC, Tsukuba, Ibaraki, Japan

A. Suzuki

Kobe University, Kobe, Japan

A. K. Ichikawa, T. Nakaya, R. Wendell

Kyoto University, Department of Physics, Kyoto, Japan

D. Brailsford, T. Dealtry, A. Finch, L. L. Kormos, M. Lawe, J. Nowak, H. M. O'Keeffe, P.N. Ratoff

Lancaster University, Physics Department, Lancaster, United Kingdom

F. Gramegna, T. Marchi, M. Cicerchia

INFN Laboratori Nazionali di Legnaro, Italy

C. Andreopoulous, G. Christodoulou, J. Coleman, N. McCauley, C. Metelko, D. Payne, C. Touramanis

University of Liverpool, Department of Physics, Liverpool, United Kingdom

T. Kutter, M. Tzanov

Louisiana State University, Dep. of Physics and Astronomy, Baton Rouge, Louisiana, U.S.A.

S. Bienstock, J. Dumarchez, C. Giganti, B. Popov

UPMC, Université Paris Diderot, CNRS/IN2P3, LPNHE, Paris, France

K. Mahn

Michigan State University, Department of Physics and Astronomy, East Lansing, Michigan, U.S.A.

G. De Rosa, G. Fiorillo, V. Palladino, C. Riccio, A.C. Ruggeri

INFN and Universita' degli studi Federico II, Napoli, Italy

M.Batkiewicz, M.Curylo, A.Dabrowska, J.Michalowski, H.Przybilski, J.Swierblewski, T.Wachala, A.Zalewska

H.Niewodniczanski Institute of Nuclear Physics PAS, Krakow, Poland

A. Ajmi, G.Collazuol, F. Iacob, M.Laveder, A.Longhin, M.Mezzetto, M. Pari

INFN and Universita' degli Studi di Padova, Italy

V. Paolone, H. Su

University of Pittsburgh, Department of Physics and Astronomy, Pittsburgh, Pennsylvania, U.S.A.

Y. Koshio

Department of Physics, Okayama University, Okayama, Japan

Y. Azuma, T. Inoue, K. Kin, N. Kukita, Y. Seiya, S. Tanaka, K. Yamamoto

Osaka City University, Department of Physics, Osaka, Japan

H. Budd, R. Flight, S. Manly, K. McFarland

University of Rochester, Department of Physics and Astronomy, Rochester, New York, U.S.A.

P. Loverre, L. Ludovici

INFN and Universita' Roma la Sapienza, Roma, Italy

F. Di Lodovico, T. Katori, S. King, R. A. Owen, B. Richards, J. Wilson, S. Zsoldos

Queen Mary Univ. of London, School of Physics and Astronomy, London, United Kingdom

Z. Chen-Wishart, A. Kaboth, J. Monroe, W. Parker, J. Walding, M. Ward

Royal Holloway University of London, United Kingdom

J.Holeczek, J.Kisiel

University of Silesia, Katowice, Poland

F. Nova, D. Wark

STFC, Rutherford Appleton Laboratory, Harwell Oxford

G. Barr, X. Lu

Oxford University, Department of Physics, Oxford, United Kingdom

C.K. Jung, C. McGrew, G. Yuang, K. Wood, Y. Wang

State University of New York at Stony Brook, Dep. of Physics and Astronomy, Stony Brook, New York, U.S.A.

H. Kakuno

Department of Physics, Tokyo Metropolitan University , Tokyo, Japan

M. Kuze

Tokyo Institute of Technology, Department of Physics, Tokyo, Japan

M. Ishitsuka

Tokyo University of Science, Dep. of Physics, Chiba, Japan

R. Fujita, K. Iwamoto, R. Tamura, M. Yokoyama

Department of Physics, University of Tokyo, Tokyo, Japan

M. B. Barbaro

INFN and Turin University, Turin, Italy

J. Lagoda, K. Kowalik, P. Przewlocki, E. Rondio, J. Zalipska

National Centre for Nuclear Research, Warsaw, Poland

M. Posiadala-Zezula

University of Warsaw, Warsaw, Poland

R. Kurjata, J. Marzec, A. Rychter, K. Zaremba, M. Ziembicki

Warsaw University of technology, Warsaw, Poland

G.J. Barker, S.B. Boyd, D. Hadley, M. Haigh

University of Warwick, Department of Physics, Coventry, United Kingdom

J.T. Sobczyk

Wroclaw University, Faculty of Physics and Astronomy, Wroclaw, Poland

Y. Asada, K.Matsushita, A. Minamino, K.Okamoto, D.Yamaguchi

Yokohama National University, Faculty of Engineering, Yokohama, Japan

The groups of the Universities of Sofia and of Uppsala have expressed interest and readiness to participate in the R&D and test beam activity, in particular for the SuperFGD, in synergy with the ESSnuSB Near Detector design study.

January 9, 2018

*Now at CERN

Abstract

The T2K experiment established the $\nu_\mu \to \nu_e$ appearance with only 10% of the original beam request of 7.8×10^{21} 30 GeV protons on target (p.o.t.). In view of the J-PARC program of upgrades of the beam intensity, the T2K-II proposal requires to run up to 20×10^{21} p.o.t., i.e. an increase of the exposure by a factor 10. The Hyper-K proposal consists in a further increase by a factor 10 of the far detector mass. Facing the potential increase of statistics by two orders of magnitude, it is of great importance to undertake a vigorous program of near detector upgrades, with the aim of reducing the statistical and systematic uncertainties at the appropriate level of 3-4% or less on the prediction of the $\nu_\mu \to \nu_e$ and $\bar{\nu}_\mu \to \bar{\nu}_e$ appearance signals in the far detector. In February 2017 the T2K Collaboration launched the program of upgrade for the off-axis magnetic near detector of the T2K experiment (ND280). This report presents a baseline proposal, which achieves a much better uniformity of acceptance as function of polar angle, by reconfiguring the geometry with a fully active scintillator detector acting as neutrino target, disposed along the plane including both the beam direction and the magnetic field. The favoured option for this detector is the Super-FGD concept, consisting of small scintillator cubes each read-out by three WLS fibers. Two new TPCs cover the large angles and time-of-flight detectors allow rejection of out of fiducial volume events. First results of performance are given showing a significant reduction of the uncertainties.

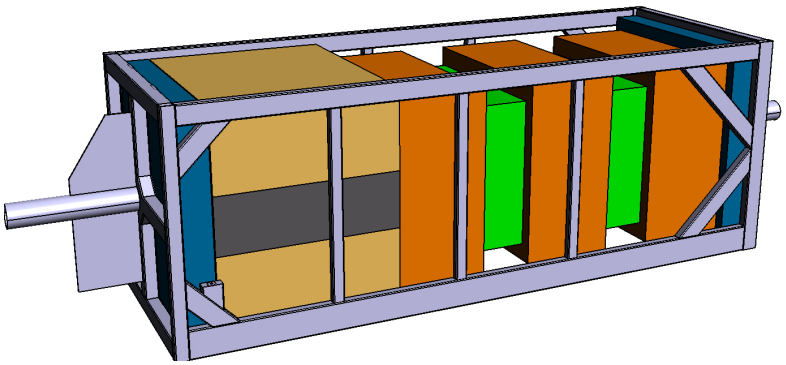

Contents

1 Executive summary

We propose to upgrade the T2K Near Detector ND280 in order to reach a systematic uncertainty at the 4% level, matching the needs of the T2K-II phase (2020-2026). This phase of the T2K experiment can provide a 3 σ exclusion of CP conservation for 36 % of the δ_{CP} phase space, around $\delta_{CP} = -\pi/2$.

We have converged on a design that significantly improves the performance provided by ND280. In particular we achieve full polar angle coverage for the muons produced in Charged Current events, improve the tracking efficiency of pions and protons stopping inside the scintillator detector and improve the electron-converted gamma separation useful for electron neutrino studies.

This is obtained with the addition of a highly granular scintillator detector. The most appealing option for this detector is the Super-FGD design (small scintillator cubes, with a $\sim$ 1 cm side, each read out with three WLS fiber). This detector is sandwiched between two High-Angle TPC, read out by resistive Micromegas detectors, with a compact and light field cage. These detectors are surrounded by six large TOF planes to determine the track direction and improve the PID. The scintillator detector will be able to track over 4π solid angle pions and protons stopping in this detector. Moreover its high granularity will allow to distinguish electrons produced by electron neutrino interactions from converted photons. The TPC will measure charge, momentum, track angles and dE/dx with excellent efficiencies and low systematics. We propose to conduct beam tests in the CERN PS East Area Hall in 2018 in order to validate these detector technologies and to ascertain their performance.

A related R&D for a High Pressure TPC (HPTPC) is also being developed, with the aim to provide a very detailed picture of neutrino interaction on the TPC gas. Several synergies between the ND280 Upgrade and this R&D have been identified both related to the detector technologies and to the physics studies. The HPTPC will be deployed in the neutrino beam in Japan on a different, later, time scale, after the design of that detector has been defined.

The construction of these detectors will provide new high quality neutrino beam interaction data useful to constrain the cross section models. Moreover, these detectors will represent a significant step forward with respect to the current state of the art, and will effectively complement other techniques for use in other Near Detectors.

We have checked the effectiveness of the new detectors with detailed simulations. Propagating the new information by the upgrade Near Detector all the way to the prediction at the T2K Far Detector, we obtain a significant improvement both with respect to a fixed neutrino interaction model, and with respect to the capability to discriminate between different models. On average, the post-fit uncertainty after taking into account the data provided by the upgrade detector will be 30% lower. Furthermore the near to far extrapolation will be much less model dependent.

The detector construction for the ND280 Upgrade will be performed in 2019-2020, for an installation in Japan in 2021.

2 Introduction

The T2K neutrino experiment at J-PARC [1] is well known for the observation of the $\nu_\mu \to \nu_e$ appearance [2], which occurs at the relatively high rate of $\sim 5\%$ of the original muon-neutrino flux. This discovery was made with only 10% of the approved proton exposure, of which the experiment has now accumulated 20%. The observation of leptonic CP violation can become accessible to the experiment, given an increase of flux and continuous efforts to reduce systematic errors. In summer 2017 T2K released the new results of the search for CP violation in the leptonic sector by directly comparing neutrino with antineutrino oscillations, based on the data taking until May 2017. The CP conserving hypothesis is excluded with a significance of 2 standard deviations [3].

The increase of statistics will come naturally from continuing running up to the full approved 7.8×10^{21} protons on target, and beyond. The proton beam power has been growing regularly and reaches by November 2017 an operational value of 455 kW. A program of accelerator upgrades is now the highest priority of KEK and J-PARC [4], with the aim of reaching a power greater than 800 kW by 2020 and 1.3 MW a few years later. The experiment has submitted a proposal for an extension of the T2K running until 20×10^{21} protons-on-target — 15 times the present exposure which has received phase-I approval. This aims at initial observation of CP violation at the 3 σ level or higher significance if the CP violation is maximal. A further increase by a factor 10 will come with the Hyper-K, increasing the far detector mass from 22.5 kt to more than 200 kt [5, 6, 7].

Much has been learned about systematic errors since 2010. They can be summarized as an uncertainty in the prediction of number of events and their energy distribution in the CC ν_μ and CC ν_e channels and background thereto, in the SK far detector, given the calculated flux and the observations in the near detector, and for any specified value of the neutrino oscillation parameters. The original design of the near detector at a time when only an upper limit on the mixing angle $\theta_{13} < 11^\circ$ was known, was made with emphasis on background reduction to the search for $\nu_\mu \to \nu_e$ appearance. Given the large signal, the emphasis shifts to systematic errors on its prediction. It is thus justified to revisit the near detector design with the benefit of experience. The present configuration leads to systematic errors of the order of 6%, the goal is to bring this number down to $\sim 4\%$ for T2K-II [8], and to $\sim 3\%$ or below for Hyper-Kamiokande.

In future measurements of oscillation parameters, a good understanding of possible biases and distortions on the energy reconstruction will become important. These stem from the fact that event reconstruction in the Water Cherenkov detector uses a kinematic formula based on the quasi-elastic assumption, which uses the final state lepton momentum and angle. Given the good momentum resolution available both in the magnetic near detector and in the fully active water Cherenkov far detector, this is quite precise, but only rigorously correct for quasi-elastic events on free protons. The presence of additional final state particles which are below Cherenkov threshold, negative pions in particular, and of nuclear effects, modifies the relationship between the reconstructed energy and that of the incoming neutrino, which is the parameter that governs neutrino oscillations. An important role of the near detector is to acquire enough information to be able to either measure directly this energy response function, or to be able to constrain the model inputs that lead to a distortion of this function.

This report is organised as follows. We first present in section 3 the upgraded near detector configuration, followed by a description of the new TPCs (Sec. 4), the scintillating detector (Sec. 5), and TOF (Sec. 6) and the plan for the test beam (Sec. 7). After presenting the integration of the new detector for what concerns DAQ and software (Sec. 8) and a related R & D for a High Pressure TPC (Sec. 9), in section 10 we discuss the studies performed to evaluate the performances of this new detector, going from Geant4 simulations to event reconstruction.

We finally conclude the proposal with some indications of the structure, schedule and next steps for this project, as well as the proposed contribution by CERN (Sec. 11).

3 The upgrade detector

3.1 Design process

The design described in this report has been developed by a dedicated team over a period of two years. First, a T2K task force studied the possible upgrade configurations while at the same time developing the software tools needed to provide a full simulation and detector response, as well as comparing the performances for each configuration. This first period ended with the task force report [9] in January 2016, endorsed by the T2K collaboration, which issued a public statement officially launching the upgrade project.

We then opened the project to the particle physicists community outside of T2K by launching a series of open workshops [10], alternating between CERN and J-PARC (Japan). In the process, we prepared and submitted to SPSC the Expression of Interest CERN-SPSC-EOI-15 [11]. This proposal embodies the studies, discussions and suggestions generated during this process.

3.2 ND280 strengths and weaknesses

In a long-baseline experiment the role of the Near Detector is to reduce the flux and cross-section uncertainties associated to neutrino production and interactions and allow a prediction of the expected spectra at the Far Detector.

One of the main strength of the T2K Near Detector ND280 (Fig. 1) is that it is a magnetized detector, providing momentum and charge determination of the leptons produced by neutrino interactions. This allows to distinguish between neutrinos and anti-neutrinos. This capability is particularly important when data are collected in anti-neutrino mode since the neutrino component in this case is large due to the larger wrong-sign flux and the larger neutrino cross-section. In addition ND280 is able to precisely measure the momentum of the charged particles produced in neutrino interactions and to perform particle identification, in particular distinguishing between muons and electrons, thanks to the presence of three TPCs and the surrounding electromagnetic calorimeter.

The main limitation that was identified in the current ND280 design is that most of the leptons are selected looking at the TPC downstream the FGD in which the neutrino interaction occurred. As a consequence the efficiency in the forward region is excellent but it drops considerably for scattering angles

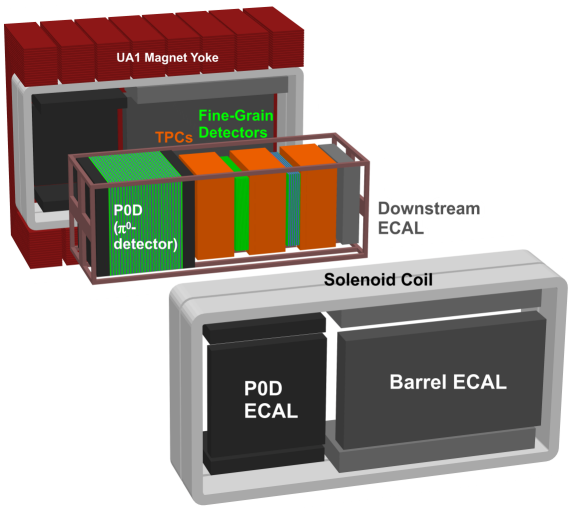

Figure 1: Exploded view of the T2K ND280 detector inside the ex-UA1 magnet, donated by CERN. The oscillation analyses use data from neutrino interactions in the Fine-Grain Detectors FGD1 (scintillator) and FGD2 (scintillator and water layers) with tracks in the three TPCs. The neutrino beam enter the detector from the left.

with respect to the beam direction larger than ~ 40 degrees. At Super-Kamiokande, instead, given the 4π symmetry of the detector, the efficiency is flat with respect to the beam direction. In the extrapolation from the expected spectra extracted using forward going tracks at ND280 to the ones at SK, cross-section models are needed to describe the dependency on the momentum transferred Q^2 or on momentum and angle.

Another limitation of the Near Detector is its poor efficiency in selecting electron neutrino interactions below 1 GeV, related both to limited efficiency for tracks at high angles, and to a contamination due to converted gammas. The method used in T2K to constrain flux and cross-section systematic uncertainties, in fact, relies on the selection of muon neutrinos at ND280 to constrain uncertainties for both ν_μ and ν_e at SK. The break-down of the systematic uncertainties at Super-Kamiokande is shown in Table 1. An additional uncertainty of 3% due to possible cross-section model differences between ν_μ and ν_e is included in the oscillation analysis and has so far a non-negligible effect on the final systematic error budget. ND280 has already measured ν_e interactions in the Tracker and in the P0D and with the current statistics and detector ability it is able to constraint the ν_e/ν_μ cross-section difference at the 10% level.

Currently this electron neutrino cross section measurement is limited by the statistical uncertainties, especially in the low energy region due to the low efficiency and large background of photons at low momentum. Even with additional statistics the low signal purity will limit the capabilities of ND280 in constraining this systematic uncertainty. An upgraded version of ND280, more sensitive to low momentum and high angle electrons produced by ν_e interactions might allow to constrain the ν_e/ν_μ cross-section ratio based on the near detector data.

In summary ND280 proved very useful to select clean sample of ν_μ and $\bar{\nu}_\mu$ interactions thanks to

Table 1: Effect of 1σ variation of the systematic uncertainties on the predicted event rates at Super-Kamiokande of the ν-mode samples [12].

Source of uncertainty	ν_e CCQE-like	ν_μ	ν_e CC1π^+
	$\delta N/N$	$\delta N/N$	$\delta N/N$
Flux	3.7%	3.6%	3.6%
(w/ ND280 constraint)			
Cross section	5.1%	4.0%	4.9%
(w/ ND280 constraint)			
Flux+cross-section			
(w/o ND280 constraint)	11.3%	10.8%	16.4%
(w/ ND280 constraint)	4.2%	2.9%	5.0%
FSI+SI+PN at SK	2.5%	1.5%	10.5%
SK detector	2.4%	3.9%	9.3%
All			
(w/o ND280 constraint)	12.7%	12.0%	21.9%
(w/ ND280 constraint)	5.5%	5.1%	14.8%

the presence of the TPCs and of the magnetic field. This allowed to reduce the flux and cross-section uncertainties at the level of 5% that is more than enough for the oscillation analyses with the statistics collected by T2K so far. With more statistics, an upgraded version of ND280, more efficient in selecting high angle and low momentum particles, as well as a larger sample of ν_e, will be necessary to achieve the physics potential of T2K-II.

3.3 Requirements for the upgrade detector

Following the considerations developed in the previous sections of this note, we can here present the requirements for the upgraded near detector:

- Full and precisely known polar angle acceptance for the muons produced in Charged Current neutrino interactions with similar performance in term of momentum resolution, dE/dx, charge measurement as the current ND280.
- Fiducial mass of at least a few tons (each of the two present ND280 targets, the FGDs, has a fiducial mass of approximately one ton).
- High efficiency 4 π tracking for low energy pions and protons contained inside the active target detector, in order to determine the event topology, with proton-pion identification.
- Good T0 determination (at the 0.5 ns level) for tracks traversing the TPCs, in order to determine their direction (backward versus forward or inward versus outward) and possibly contribute to the

particle identification.

3.4 The new detector configuration

The reference detector design is schematically shown in Fig. 2. It modifies the current ND280 configuration only in the upstream part and retains all other detectors except the P0D central part. Proceeding along the neutrino beam direction, after the Upstream ECal P0D (lead scintillator sandwich, 4.9 X_0), we introduce a sandwich of a high granularity Scintillator Detector (SD) of approximately 2 ton, with two Horizontal TPCs (referred to as High Angle TPC, HA-TPC, in the following), one above and one below. This central block of detectors is surrounded by a thin layer of TOF detectors, mounted in front of the large angle P0D ECAL.

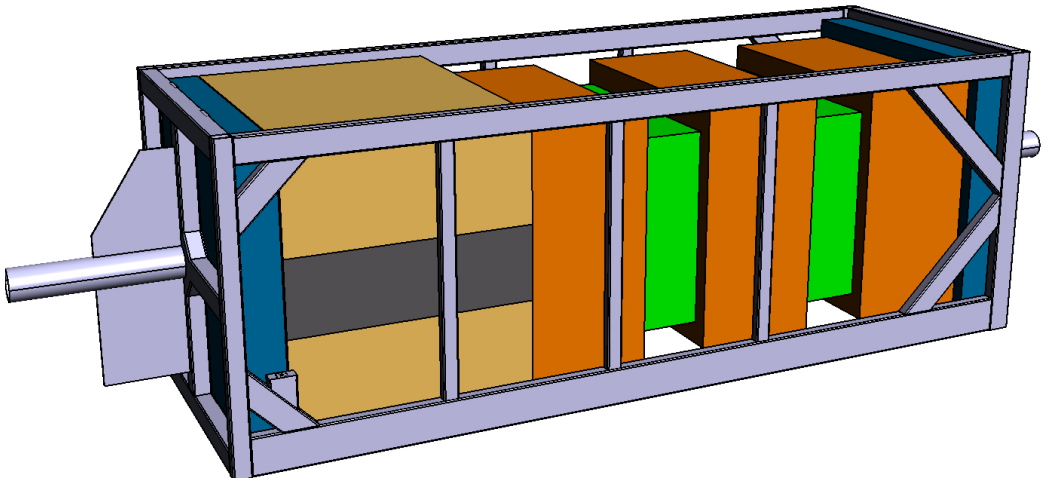

Figure 2: Schematic of the upgrade ND280 detector in the basket. The two new High Angle TPCs (light brown area) as well as the new scintillator detector SD (grey area) are shown on the left hand side. Neutrinos enter the detector from the left. The axis are defined in such a way that x is along the magnetic field direction, y is in the vertical direction and z is along the neutrino beam direction (i.e. the longer axis of the detector structure).

Charged particles produced in neutrino interactions in the SD will be tracked inside this detector. Those exiting SD will traverse a system of TPCs disposed around them, achieving an almost full polar angle coverage.

The downstream part of ND280 will be kept untouched. It will therefore serve as a reference for comparing future interaction rate measurements to those obtained in T2K-I. Keeping these detector in place will also minimize the installation personnel and time and will avoid the risks intrinsic in moving the detectors to a different location inside the basket.

An important advantage of the upgraded detector, as it will become evident later, is it larger instrumented mass, almost doubling the present mass of the two FGDs. Even more important, the upgrade will provide several new samples for the oscillation fit. This comprises a sample of interactions in the new SD with the muon in TPC1 (new forward sample) as well as a sample of interactions where the muon

enter the HA-TPC above or below. The latter sample contains muons in the forward direction, around 90 degrees, and backward. These samples provide a significant polar angle coverage, while at the same time having significant overlap with the present FGD1 samples.

The higher tracking performances of SD and the better timing will also provide significant improvements in the physics performance.

3.5 TOF counters

One of the problem of the present ND280 configuration is that, while low momentum backward particles are reconstructed in the TPC, it is also necessary to determine the direction of the track and this requires at least two hits in fast scintillation detectors. To overcome this problem we plan to surround the new HA-TPCs with scintillator detectors for TOF determination.

The determination of the direction of tracks (backward vs forward or inward vs outward) requires only a modest time resolution as the two hypotheses are typically separated by 6 ns for a 1 m track length. However sub-nanosecond time resolution opens the interesting possibility to complement TPC PID with TOF. For instance the TOF of a proton is 5.4 ns (1.5 ns) larger than for a positron over a distance of 1 m for 0.5 GeV/c (1 GeV/c). This will be useful for $\bar{\nu}_e$ where the overlap between the dE/dx curves for protons and positrons is a potential problem.

3.6 Calorimeters

Concerning the calorimetric coverage, we plan to keep in place both the downstream calorimeter and the barrel calorimeters. The calorimetric coverage is excellent in the downstream basket region. Here the calorimeter has a thickness of 10 (11) radiation lengths for the barrel (downstream) region and has good segmentation.

In the upstream basket region (2.2 m in z starting from the upstream part of the basket and corresponding to the current P0D) the calorimetric coverage is performed with 4.3 X0 and a much coarser segmentation provided by the ECAL-P0D. We are currently evaluating whether this calorimetric coverage is sufficient for the physics program of T2K-II or if some improvements are needed. We notice however that at the moment the ECAL information is used only for ν_e analyses (where it helps the rejection of muons) and to tag photons (to increase the purity of the CC0Pi sample).

4 High Angle TPCs

4.1 Introduction

The combination of thin active targets made of scintillators and TPCs inside the magnetised volume of the UA1 magnet is the distinctive feature of the current T2K off-axis near detector ND280. All the T2K oscillation analyses use as a constraint on the neutrino flux and cross-sections the data from these detectors.

The TPCs [13] have been particularly useful because they provide several crucial informations for the event reconstruction and the analysis:

- track reconstruction in 3D. All other detectors have coarser granularity and projected position information (mostly the in the x or y directions). Therefore TPC tracks are used as pivot in the reconstruction.
- charge measurement;
- momentum measurement;
- particle identification by combining dE/dx with momentum measurement.

We would like to maintain all these key features in the upgraded detectors and therefore plan to build new TPCs with performances substantially similar to the performances of the existing TPCs.

Another key consideration is the fact that TPC are especially well suited to track low momentum tracks as those produced in neutrino interactions with the T2K off-axis beam: from a few GeV/c in the forward region, to a few hundred MeV/c in the high angle and backward regions.

4.2 Design consideration and required performances

The performance obtained with the existing TPC has been completely satisfying and no substantial improvement is needed. The requirement on the momentum resolution is rather loose, 10% at 1 GeV/c. Indeed, when reconstructing the neutrino energy, the lepton momentum is used in the Charged-Current Quasi-Elastic hypothesis : in particular the initial state nucleon is supposed free and at rest. The effect of the Fermi momentum (of the order of 200 MeV/c) introduces a smearing in the relation between the neutrino energy and the lepton momentum of the order of 10% at 1 GeV/c. The requirement on the momentum resolution translates into a space point resolution around 800 μm for a magnetic field of 0.2 T, 72 space points and a track length of 72 cm in the forward region (Fig. 3).

The requirement on the momentum resolution is easily satisfied in the high angle and backward direction, where tracks have lower momenta, around 500 MeV/c and down to 200 MeV/c.

Another important requirement is related to the separation of electrons from muons for the measurement of the ν_e cross-section. Since the ν_e flux represents only approximately 1 % of the total neutrino flux, an excellent e-μ separation is needed and the TPC particle identification is crucial to this task. We have achieved in the existing TPC a resolution of 8% on minimum ionizing particles for the dE/dx measurement and this performance is sufficient for the ν_e studies [14], providing approximately 4 σ separation between electrons and muons (Fig. 3). As the resolution on dE/dx is largely driven by the track length L (the dependence is roughly $\sigma \propto 1/\sqrt{L}$), we conclude that we also need a measured track length of approximately 70 cm in the vertical direction.

The performance required for track position and angles is not critical. Indeed, what matters is a good matching between a track in the TPC, and either a track or hits in the Scintillator Detector, with a typical resolution at the few mm level.

Following these considerations, the design of the new TPCs is mainly based on the design of the existing TPCs with two major changes:

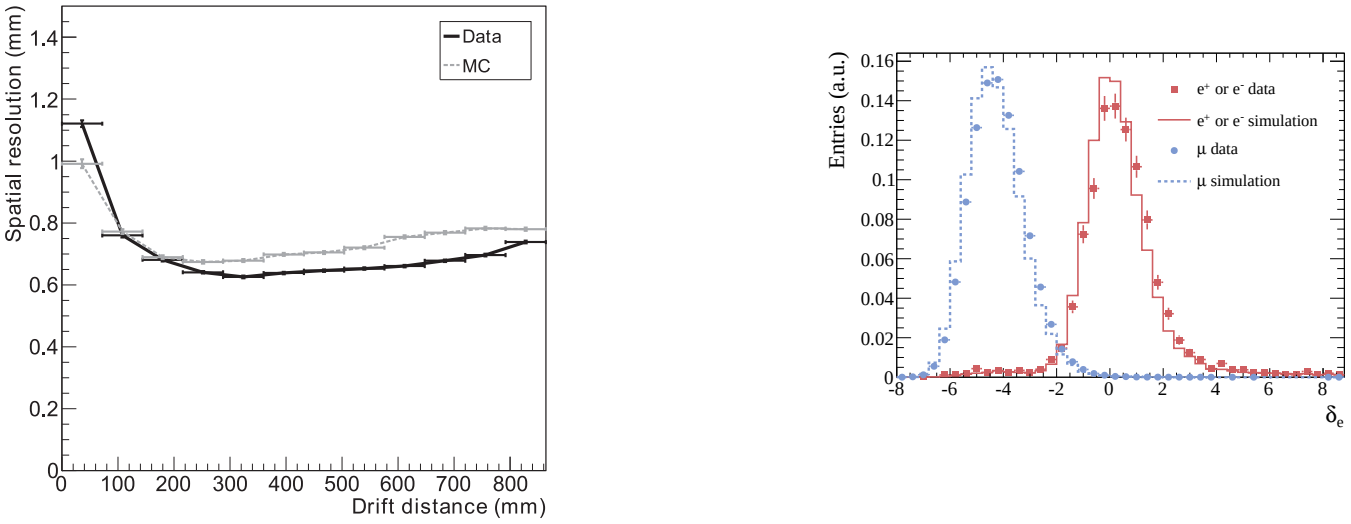

Figure 3: Left: space point resolution for the existing ND280 TPC as a function of the drift distance [13]. Right: Pull in the electron hypothesis of the TPC dE/dx for a control sample of electrons (red) and muons (blue), together with the MC predictions [14].

- the Micromegas detector will be constructed with the "resistive bulk" technique, that naturally introduces a spread in the charge on the anode plane, thereby allowing in principle a lower density of readout pads. This technique allows also to eliminate the discharges (sparks) and therefore the protecting diodes on the front end cards are no longer necessary.
- The field cage will be realised with a layer of solid insulator mounted on a composite material. This will minimize the dead space and maximize the tracking volume.

A schematic view of a HA-TPC module is presented in Fig. 4.

The parameters of the High Angle TPC (HA-TPC in the following) can be found in Table 2. They are intended as a first step of the design and not as final values.

4.3 Field Cage

The TPC is made out of a gas containment box equipped with field-forming strips and a readout plane holding several MicroMegas (MM) modules (Fig. 4). In the context of this document, *field-cage* indicates the box and its electrostatics elements, excluding the readout modules and its support structure (called end-plate).

The required electric field uniformity must be good enough to guarantee distortions in the reconstructed position of charge deposits that are small enough not to affect the momentum scale by more that 2% ; the design of electrostatic elements will be validated by ANSYS simulations at INFN-Bari, also making sure that the geometry of the corners of the HA-TPCs will be optimized to avoid high electric fields in these regions.

The new TPCs differ substantially from the existing ones not only by their placement and orientation,

Table 2: Main parameters of the HA-TPC.

Parameter	Value
Overall x - y - z (m)	2.3 - 0.8 - 2.0
Drift distance (cm)	90
Magnetic Field (T)	0.2
Electric field (V/cm)	275
Gas AR-CF_4-iC_4H_{10} (%)	95 - 3 - 2
Drift Velocity $cm/\mu s$	7.8
Transverse diffusion ($\mu m/\sqrt{cm}$)	265
Micromegas gain	1000
Micromegas dim. z-y (mm)	340 - 410
Pad z - y (mm)	11 - 11
N pads	36864
el. noise (ENC)	800
S/N	100
Sampling frequency (MHz)	25
N time samples	511

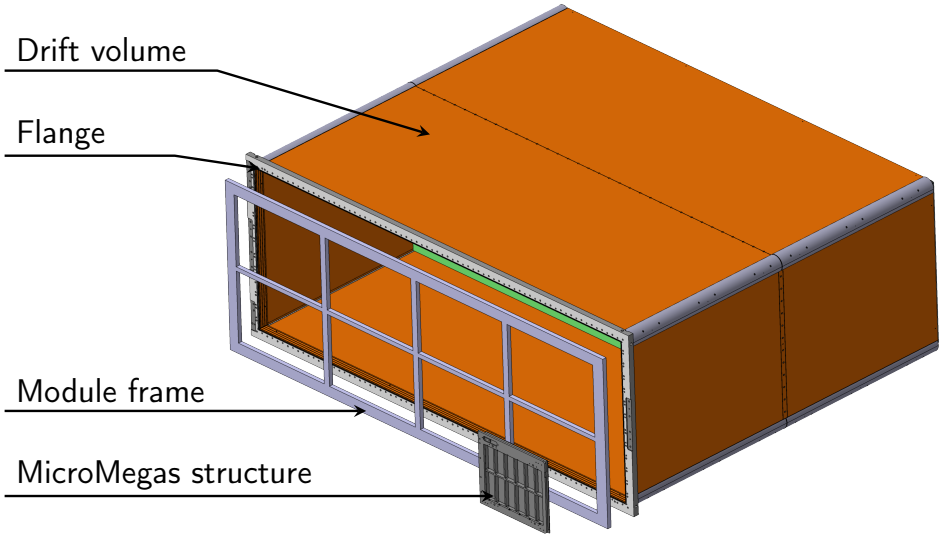

Figure 4: Schematic view of the High-Angle TPC.

but mainly by the need to maximize the acceptance for large angle tracks. This is achieved by reducing the dead region around the sensitive gas volume and the amount of material surrounding it. The design goal can be fulfilled by adopting a single-volume configuration where the function of gas containment and electrostatics are combined in one single structure. We have set the goal that the total material budget should be smaller than 2% of a radiation length.

4.3.1 Challenges

The gas amplification technique and the drift length will be very similar to the ones of the VTPCs, and there is no reason to change the composition of the active gas mixture Ar:CF_4:iC_4H_{10} (95:3:2). This mixture provides high speed and moderate diffusion even at moderate values of magnetic and electric fields. In these conditions the field cage has to stand moderate ($\approx 25kV$) central cathode voltages and guarantee *normal* (i.e. $\lesssim 10ppm$) levels of oxygen impurity - but not extreme ones.

The acceptance and material requirements can therefore be satisfied by a single-wall field cage, knowing that the design of the walls will depart substantially from that of the existing ND280 TPCs:

- The outer field-cage and outer gas CO_2 gas volume of the existing ND280 TPCs has the functions of taking most of the overpressure of the gas and insure the electrical insulation. The advantage of this approach is that even in the case of a discharge, no permanent damage can be produced in

layer of the wall	d [cm]	X_0 [cm]	d/X_0 [%]
copper shielding	0.001	1.45	0.07
polyimide substrate	0.005	32.65	0.02
outer GRP	0.03	15.79	0.19
aramid paper	0.007	29.6	0.02
honeycomb	2.35	1383	0.17
inner GRP	0.03	15.79	0.19
polyimide insulation	0.0125	32.65	0.04
mirror strips	$0.8 \cdot 0.0035$	1.45	0.19
polyimide substrate	0.0050	32.65	0.02
field strips	$0.8 \cdot 0.0035$	1.45	0.19
epoxy glue	$\approx 6 \cdot 0.007$	≈ 35.2	0.12
		$\sum$	1.21

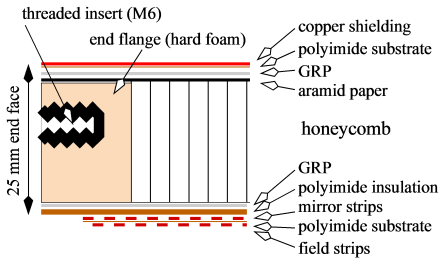

Figure 5: Left: material budget for the ILC-TPC field cage. Right: cross-section of the field cage and interface to the end flange.

contrast to the case where a solid is used for the HV insulation. On the other hand a significant disadvantage of the dual volume approach is the introduction of an additional, non-negligible dead space of about 8 cm between the target and the sensitive volume. The walls of the HA-TPCs will provide both functions: this is certainly doable, but requires a careful study.

- The field-forming strips of the existing ND280 TPCs are laid on the panels of the inner field cage, which is not subject to significant mechanical stresses. In the case of the HA-TPCs the strips will be made on the inner side of the single-wall structure: any mechanical deformation will induce non-homogeneous regions of electric field and must therefore be kept under control.

4.3.2 Possible technical solutions

Several composite materials are being considered for the field cage walls, the most straightforward one being G10-clad honeycomb panels. This material is well known for the construction of TPC panels; it has been used for the VTPCs and is considered for future TPCs, including those studied for the ILC detector ILD. The mechanical robustness of possible wall structures has been simulated with respect to mechanical and thermal stress by an engineer at IFAE using a Finite Element Analysis Software package optimized for this purpose. Samples for testing and the walls for the prototype and the final TPCs will be build either with an autoclave at INFN Padova or a company from Spain.

The wall panels will be separately produced and then mounted on a rectangular support structure made of G10 or Kevlar. This structure also will serve to install the flange on which the end plate will be mounted. Stability studies of this structure will also be performed.

Two different schemes are being considered for making the set of the conductive strips on the inner face of the walls.

- The first option is derived from the design of the ILC TPC [15]. The honeycomb panel is layered with a set of field strips and mirror strips, separated by a polyimide film. The typical size of the strips is of the order of the mm. This scheme gives the smallest possible region of non-uniform field but comes at the cost of additional complication in the connection of the underlying mirror strips

Figure 6: Possible configurations for the case of double sided copper strips.

to the voltage divider. This configuration and the corresponding material budget is shown in Fig. 5. Two possible configurations for the double sided copper strips are shown in Fig. 6.

- A mechanically simple alternative comes from the design of the HARP TPC [16]). The scheme is also based on a set of field and mirror strips, but while the mirror strips are glued on the mechanical structure, the field ones are made of aluminized mylar strung over a thin mechanical support. This technique makes it easier to connect both sets of strips to the voltage divider, but it implies a larger step (order of the cm) and therefore a larger amount of active volume affected by edge effects in the electric field.

Combined mechanical and electrostatics simulations will allow to choose the best compromise in terms of acceptance and cost of the field cage.

4.4 Micromegas for the readout plane

Micro-Pattern-Gas Detectors have been successfully used in a variety of particle physics experiments in the last two decades. They offer distinctive advantages in TPC with respect to wire chambers: while providing good gas amplification they induce only minor non-uniformities of the electrical field (due to the E $\times$ B effect), substantially reduce the ion back-flow in the drift volume, and are free from the long-term aging and mechanical constraints affecting wire chambers. They are therefore suited to paving large surfaces with minimal dead regions.

The performance of the ND280 TPCs, the first large TPC built with MPGD, has in this respect been excellent. Since their installation in 2009, the 72 Micromegas are performing according to the specifications, without degradation of their response and without failures.

4.4.1 Resistive Micromegas

The ILC TPC has succesfully tested a new kind of detector, the resistive Micromegas [17]. A schematic cross-section view of this device is shown on Fig. 7.

The pads are covered by a layer of insulating material and then by a layer of resistive material. An avalanche is then naturally quenched because the potential difference locally drops in presence of a high charge density. The resistive layer acts like a 2-D RC network and the charge deposited by the avalanche spreads naturally with time with a Gaussian behaviour. For a point charge deposited at $r = 0$ and $t = 0$, the charge density as a function of radius r and time t reads

$$\rho(r,t) = \frac{RC}{2t} e^{-r^2 RC/(4t)} \quad (1)$$

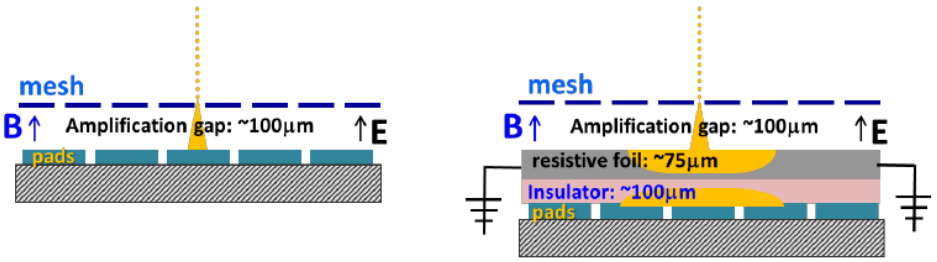

Figure 7: Schematic cross-section of a normal bulk Micromegas (left) and a resistive Micromegas (right). The pads are covered by a layer of insulating material and a layer of resistive material.

where R is the resistivity per unit area and C the capacitance per unit area.

In this way, even for small drifts, when the electron cloud width is low, the resistive layer will enable the charge to be detected over several pads. In the ILC TPC this configuration allowed to reach excellent spatial resolution of 70 μm even for small drifts. Examples of the Pad Response Functions (PRF) measured in ILC-TPC prototypes are shown in Fig. 8.

In our case, this device will allow a readout structure with large pads, without compromising the space point resolution. In addition, the natural quenching properties naturally suppress Micromegas discharges (so-called sparks) and therefore no protection diodes are required for the front-end electronics.

We plan to use for the resistive layer a kapton (polyimide) foil, on which a layer of Diamond-like-Carbon has been deposited by sputtering. The resistivity can be tuned by increasing the thickness of the carbon layer, and by doping the carbon with nitrogen. The aim is to use a resistivity of 1 MΩ/square.

Several resistive Micromegas are in the fabrication process to validate this technology, some of which will be produced by the CERN EP/DT MPGD workshop. They will be tested in the next months with cosmic rays in the Saclay laboratory.

4.4.2 The readout plane

A sketch of the TPC readout plane is presented on Fig. 9. Each readout plane will be composed of eight Micromegas modules of approximate dimensions 34 $\times$ 41 cm^2. Each Micromegas will be segmented in 32x36 pads of dimensions 1.06 $\times$ 1.13 cm^2.

4.4.3 Test bench for the production of the Micromegas detectors

The test bench for the HA-TPC Micromegas detector is mainly used to qualify the gain and performances and to provide an absolute calibration for the signals detected by the TPC. The architecture of the test bench will be similar to the one used in the T2K experiment in 2008 [18]. Each produced Micromegas will be mounted on this setup and thoroughly tested. A robotic arm equipped with a 55Fe source will be used to provide a narrow, collimated beam of X rays generating an input signal for each pad of the detector. The scan of the whole detector in the XY directions will provide the following information: uniformity, dead pads, gain map and energy resolution. As the X-ray conversion region will be narrow it

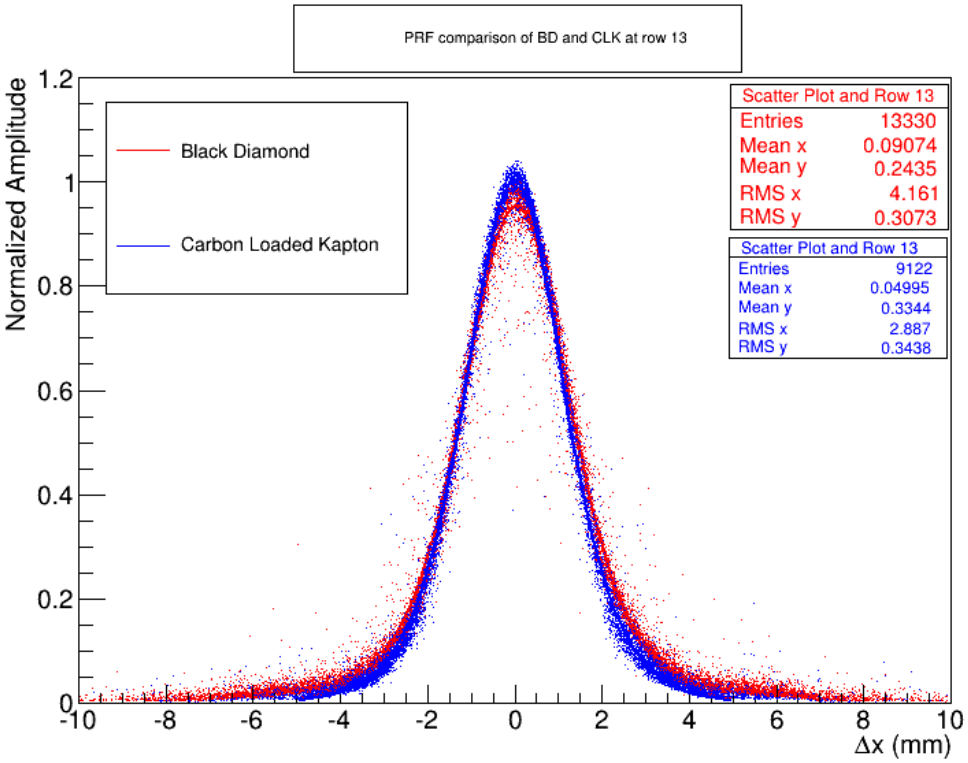

Figure 8: Pad Response Function (PRF) for two types of resistive Micromegas tested by the ILC TPC collaboration with a resistivity of 5 MΩ/square.

will be possible to measure the spread of the signal and verify the spatial resolution, which is an important factor, especially with resistive Micromegas detectors.

4.5 TPC Electronics

The readout system of the HTPC is conceptually very similar to that of the existing TPCs [19]. Differences, technical improvements and simplifications are outlined below.

4.5.1 Readout architecture

The architecture of the readout system of the HTPC is schematically shown on Fig. 10. It is based on the replication of the modular structure used to read out each Micromegas detector module. The front-end electronics is composed of two types of electronic boards: the Front-End Cards (FEC) capture the analog signals of the pads of each detector module and convert the acquired samples in digital format using a fast multi-channel analog to digital converter (ADC). Elementary data processing such as baseline offset correction, zero-suppression and temporary storage is performed by the Front-End Mezzanine card (FEM) which is connected to the number of FECs required to read out one detector module. In order to minimize the degradation of the highly sensitive detector analog signals and avoid the high cost of cables, the FECs and the FEM are directly mounted at the back of detector modules, as it is done for the existing TPCs. The data of each detector module is transported outside of the detector magnet

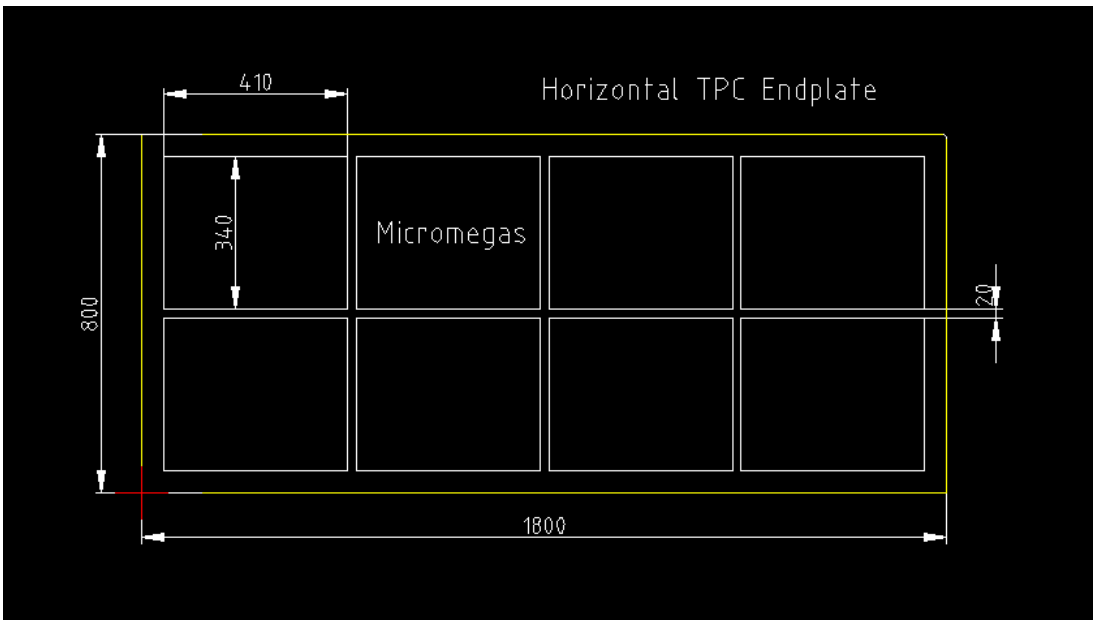

Figure 9: Schematic view of the TPC module frame supporting eight Micromegas modules.

via an optical fiber to a back-end unit that aggregates the data of multiple modules and distributes the global clock and common trigger signal to the front-end electronics using the return path of the optical link. Each back-end unit is connected via a standard Gigabit Ethernet point-to-point link to a control PC that bridges the HTPC readout system to the global run control and data acquisition system of the nd280m detectors. Alternatively, the back-end units may be connected directly to the local area network of nd280m provided that they run directly the data acquisition programs based on the MIDAS framework used by the experiment.

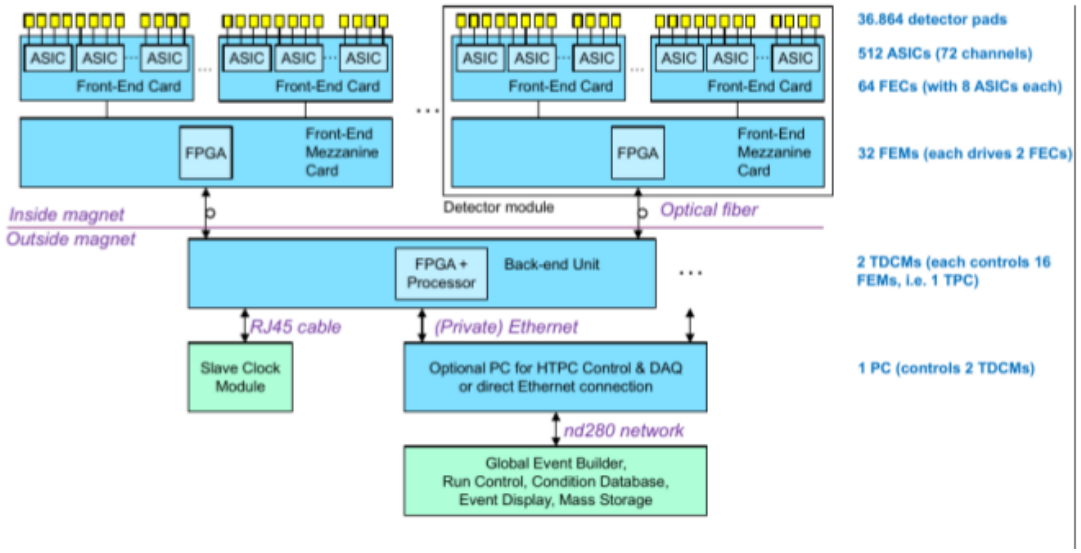

Figure 10: The architecture of the readout system of the HTPC.

4.5.2 Front-end electronics

Readout ASIC

Several options have been considered for the readout ASIC of the HTPC: the AFTER chip [20], designed for T2K and used in the current TPCs and FGDs, its successor, the AGET chip [21][3], or a derivative, the DREAM chip [22]. However, the improvements and additional features of these newer devices would not bring any real benefit compared to the original AFTER chip given the requirements of T2K. Therefore, we propose to build the readout system of the HTPC around the AFTER chip, which is a proven solution. The remaining stock of encapsulated and tested AFTER chips is 700 units (i.e. 50,000 channels) which is expected to be sufficient for the project. If required, more chips could be produced, but extra time and resources would be needed in that case, and the obsolescence of the plastic encapsulation used for the original AFTER chip is an issue that would need to be solved.

Front-End Cards

The FECs support the AFTER chips that amplify detector pad signals and sample them in an analog memory (511-bucket switched capacitor array) which is digitized by a commercial 25 MHz 12-bit ADC when a trigger occurs. Assuming that resistive Micromegas detectors are used, the number of channels per detector module will be reduced compared to the current TPCs (e.g. from 1728 pads to 1152 pads) and the anti-spark protection circuit currently used on every channel will no longer be needed. We expect that the corresponding reduction in channel count and board area for passive components will allow a sufficient reduction of the size of the FECs to mount them parallel to the detector sensitive plane instead of the significantly less compact perpendicular orientation used on the existing TPCs. We also plan to double the number of AFTER chips per front-end card from four to eight, so that only two 576-channel FECs per resistive Micromegas detector module will be required instead of the six 288-channel FECs used for the metallic Micromegas detectors of the current TPCs.

Front-end Mezzanine Cards

Each FEM performs the data aggregation of the two FECs of a detector module. A mid-range FPGA, coupled to a memory buffer and ancillary logic, implements all the required functions and interfaces to the back-end electronics via an optical fiber link. Compared to the FEM of the existing TPCs, the FEM for the HTPC controls two FECs (double density) instead of six and no longer includes a dedicated microcontroller and CANbus slow control network. This simplifies design, development and maintenance. Current, voltage and temperature monitoring on the new FEM is controlled by the local FPGA and monitoring data is time multiplexed over the optical link along with detector data. Assuming that the two HTPC are composed of two end-plates of eight detector modules each, the corresponding readout system comprises 32 detector modules, 32 FEMs and 64 FECs.

4.5.3 Back-end electronics

The back-end electronics is composed of several units which control multiples FEMs and interface to the data acquisition system of the experiment through an intermediate PC, or directly. Each back-end unit is an electronic board composed of a commercial System-On-Module plugged on a custom made carrier

board. The carrier board also includes a plurality of optical transceivers to connect to the front-end. The physical layer of the optical links may be placed on a mezzanine card that plugs on the carrier board of the back-end unit. This structure is adopted for the general purpose "Trigger and Data Concentrator Module" (TDCM) currently under development for multiple projects, possibly including T2K. A newer improved version could also be built. The current TDCM uses the powerful Mercury ZX1 module [23] from Enclustra based on a Xilinx ZYNQ FPGA that integrates a multi-core 800 MHz ARM processor (Fig. 11). The TDCM supports up to two 16-optical port mezzanine cards. A TDCM with only one 16-port optical link mezzanine card would be adequate to read out each HTPC, i.e. the complete system would require two TDCMs. The primary 100 MHz clock and the common trigger signal is provided to the back-end modules by the Slave Clock Module (SCM), a board currently used in nd280m.

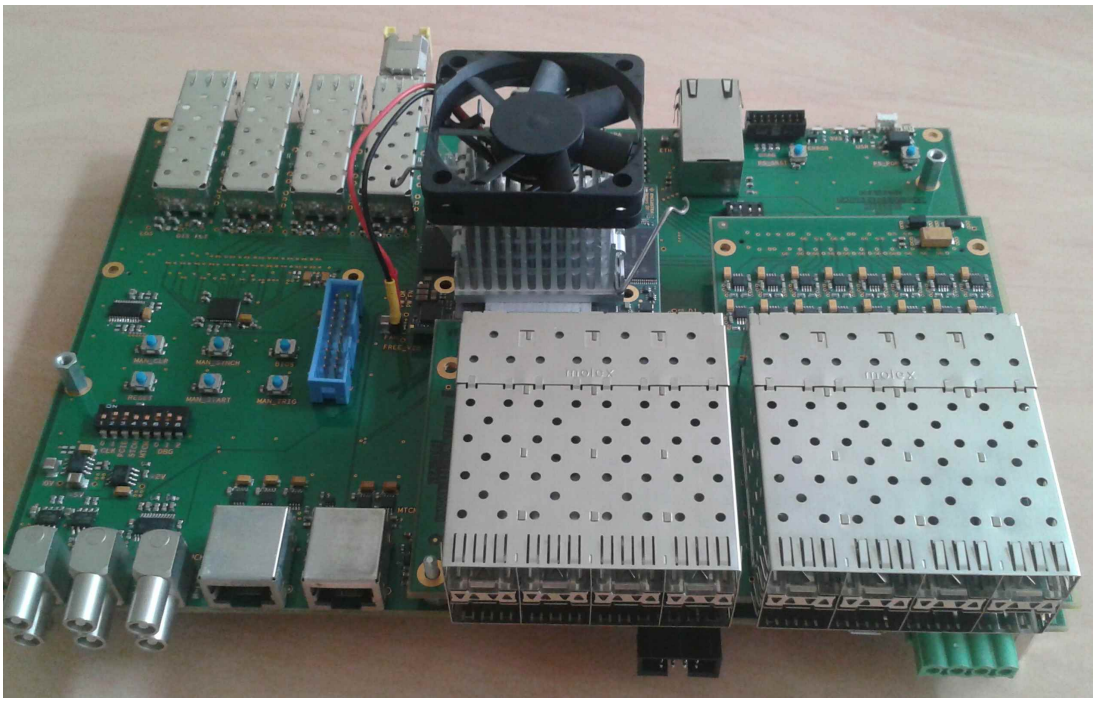

Figure 11: Prototype of the backend card using a Xilinx ZYNQ FPGA.

4.5.4 Control and data acquisition software

Two options are being considered for the control and data acquisition software. In the first scheme, which is unchanged compared to the existing TPCs, the processor of the back-end units execute a simple "bare-metal" command interpreter program and an intermediate PC running the MIDAS framework performs the translation between the global data acquisition system and the HTPC sub-system. In the second scheme, which is currently deployed in the FGD, the processor of the back-end units run the Linux operating system and execute MIDAS processes locally so that the connection of the HTPC to the common data acquisition of the experiment is made directly. There are pros and cons to each scheme.

4.5.5 Ancillary services

Because the HTPC will have less channels than the existing TPCs, power requirements will be reduced. Instead of bringing a high current 5V supply to the front-end modules, we plan to transport a higher voltage, e.g. 12 V or more, over cables of significantly smaller cross section and perform efficient power conversion locally using DC/DC converters. Finding a solution usable in a 0.2 T magnetic field needs further studies. We anticipate that the total power consumption of the front-end electronics of the two HTPC will be 640 W (e.g. 4 V x 160 A). Because the front-end electronics is placed in a confined space, water cooling is necessary. Using bi-directional optical transceivers instead of optical transceivers that require different fibers for the transmission and reception path allows halving the number of optical fibers.

4.5.6 Test-benches

Test bench for the production of the Front-end Cards

The role of this test stand is the quick validation of every FEC at the end of the assembly line: verification of all input channels, assessment of the noise level and measurement of the crosstalk level between neighbouring channels. Calibration pulses will be injected with the built-in pulser of the FEC. A custom PCB will make a capacitive load representative of a Micromegas detector. The test bench will also consist of a validated FEM and a portable DAQ computer. A user-friendly interface will allow a non-expert technician to run a pass or fail test at the production factory. Detailed tests and the analysis of eventual defaults will be performed by the designers of the FEC in a laboratory environment.

Test bench for the production of the Front-end Mezzanine Cards

This test stand is required for the validation of every FEM at the production site. All the analog and digital functions and interfaces of this card have to be tested. Using the appropriate dedicated software on a small DAQ computer, a technician at the board factory will run a pass or fail test. Deeper analysis will be conducted by the designers of the FEM if that is needed.

4.6 Gas system

The existing TPCs were designed to operate with a full volume change of gas every six hours, meaning that gas is supplied to each TPC volume at a rate of 10 L/min, for a total of 30 L/min for the three TPCs. This rate is set by diffusion of O_2, CO_2, and H_2O into the TPCs. The 30 L/min comes from 27 L/min of recirculated gas that goes through molecular sieves to be purified, and 3 L/min of new gas.

The pressure control is made with a pump operating at a constant 55 L/min and a flow controller that operates at 25 $\pm$ 2 L/min to keep the chamber pressure relative to atmosphere relatively constant. This flow controller can be adjusted to operate at 10 $\pm$ 2 L/min to allow the input flows to TPCs to be increased to 45 L/min. Then when there are five TPCs in the upgraded ND280, the flow rate to each of the TPCs will be 9 L/min.

Then 45 L/min to the TPCs will be supplied from 40.5 L/min of recirculated gas that goes through the molecular sieves and 4.5 L/min of fresh gas. With this increased fresh gas flow, the argon supply cylinders would have to be changed every 6 days (rather than every 10 days) during normal operation.

The minimum modifications to the existing system that would be to add two additional mass flow controllers, bubblers and manual flow rotameters. The manual flow rotameters are for the "standby" gas flows of Ar at 250 cc/min per chamber. The stand-bye flow is through the CO_2 gap and TPCs and currently totals 1.5 L/min, which would increase to 2.0 L/min with the addition of 2 TPCs without CO2 gaps.

Additional gas lines would have to be plumbed to the new TPCs, and additional space in the gas racks would need to be found for the flow controllers and bubblers. Alternatively we may need additional space on the SS level for a new gas rack for the new components.

Finally the Programmable Logic Controller (PLC) would have to be modified for the new Mass Flow Controllers. The existing system was programmed by the TRIUMF controls group. It is a Modicon Quantum IEC processor, and the PLC code is written in Concept (IEC programming).

A possibility that we are currently investigating is that the gas system is rebuilt on the basis of the CERN EP/DT standard. This will require replacing the mixer, flow control, purifiers with standard units provided by CERN together with the corresponding PLC control units.

In either cases, in order for this modification to succeed, the new TPCs will be in the same control loop as the existing TPCs, and would see similar pressure variations of 0.4 ± 0.1 mbar.

At startup, the detector volumes need to be purged with the correct gas mixture. The existing mass flow controllers for the purge can supply a maximum of 31 L/min, and are already operated at 30 L/min during the purge. The current purge takes 24 hours for 4.5 full purges, and uses 6/10 of the banks of Ar. With two additional TPCs this purge would take 40 hours, and use 9/10 of a bank of Ar.

In summary, modification of the existing gas system should be possible for an ND280 upgrade that would include two new TPCs of similar volume to the existing TPCs.

4.7 Prototype

We plan to construct a TPC prototype in 2018 to serve as a test facility to develop the production process and to verify the results obtained with simulations and mechanical test samples for the field cage. It will also provide a full system test and detailed tests of the resistive Micromegas. It will be a mandatory step towards the final HA-TPCs. The prototype TPC will be a single sided TPC with a maximal drift distance of 80 to 100 cm, comparable to the one of final TPCs. The xy dimensions of the module frame will allow to host one or two Micromegas modules. Suitable magnets comprise the 1T magnet available at DESY and the HARP magnet. The requirement to be able to install the TPC prototype in one of these magnets limits the xy dimensions to about 57x57 cm. The production of the prototype will start spring 2018. The test beam setup will be described in a following section.

5 Scintillator Detector

5.1 Introduction

The Scintillator Detector (SD) will act as the target for the neutrino interaction as well as the detector to reconstruct the tracks around the interaction vertex. It needs to have:

- sufficiently large mass to provide a sufficient number of neutrino interactions (comparable to the total mass of the current FGD, 2 tons)
- acceptance for charged leptons (muons and electrons) from charged current interactions that matches the surrounding TPCs
- capability to reconstruct and identify short tracks of low energy hadrons around the interaction vertex.

As described earlier, the dimensions of the SD under consideration is approximately 1.8 m(W) $\times$ 2.0 m(L) $\times$0.6 m(H), corresponding to about two tons of target mass for neutrino interactions. The detector will be based on plastic scintillators read out via wavelength shifting fibers, which is a technology commonly used for the existing ND280 detectors except for TPCs. Considering the importance of detection of low energy hadrons and the target mass, the current focus of the detector design is a fully active scintillator target detector.

5.2 Detector configuration

There are several designs under consideration for the target detector. Each of them has different properties such as performance, matureness of technology, and prospective cost. R&D is ongoing to establish the feasibility and to evaluate the performance, for both hardware and software aspects. The selection of the final design is expected to be made after evaluating the performance, feasibility and available resources. A brief description of the two designs is given below.

5.2.1 Super-FGD

Recently, a novel idea of a fine grained fully-active plastic scintillator detector made of many optically independent cubes was proposed by members of this proposal [24]. The detector design, called Super-FGD, consists of many cubes of extruded scintillator read out along three orthogonal directions by wavelength shifting (WLS) fibers (Fig. 12). The candidate scintillator is a composition of a polystyrene doped with 1.5% of paraterphenyl (PTP) and 0.01% of POPOP. The cubes produced by Uniplast, a company in Vladimir, Russia, are covered by a $\sim 50\mu$m thick chemical reflector, obtained by etching the scintillator surface with a chemical agent that results in the formation of a white micropore deposit over the polystyrene [25]. Each cube has three orthogonal cylindrical holes of 1.5 mm diameter drilled along X, Y and Z axes. Three 1.0 mm diameter WLS fibers are inserted through the holes.

Table 3 shows possible parameters of the detector and scintillator cubes. The current R&D is based on the design of 1$\times$1 cm^2 cube. If this design turns out to be difficult to achieve (e.g. due to large number

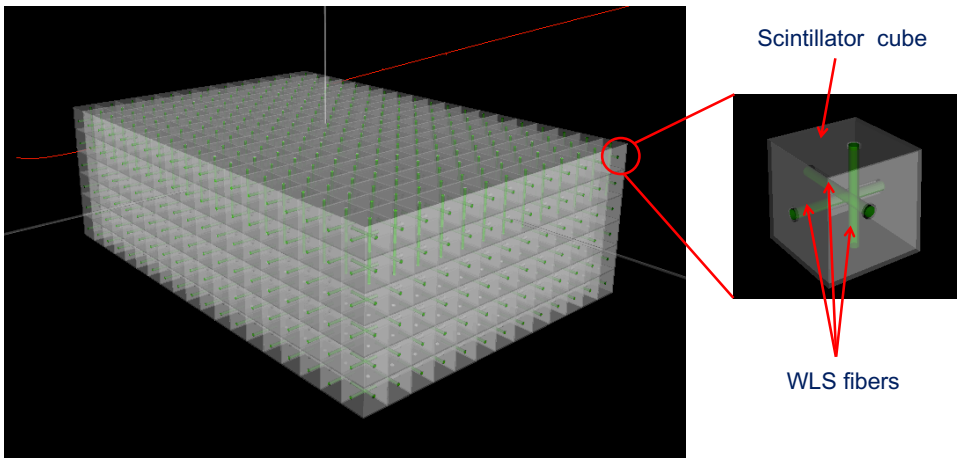

Figure 12: Schematic of the super-FGD structure.

Table 3: Main parameters of the super-FGD configuration of the size of $1.8 \times 0.6 \times 2.0$ m^3.

Parameter	Cube edge: 1 cm	Cube edge: 1.5 cm	Cube edge: 2 cm
# of cubes	2,160,000	638,400	270,000
# of channels	58,800	26,080	14,700
Total fiber length	65 km	29 km	16 km

of channels), a possible alternative option is to enlarge the size of the cube to 1.5×1.5 cm^2 or 2×2 cm^2, which could drastically reduce the number of cubes and readout channels at the risk of granularity. A picture of a small prototype is shown in Fig. 13.

The properties of the scintillator cubes have been measured in INR Moscow. Figure 14 shows the measured dimensions for the first 166 cubes. The size was measured for three directions and all are plotted together. The mean and sigma are measured to be 1004.2 μm and 75 μm, respectively, for this set of cubes. A production of 10,000 cubes is in progress to study the mechanical issues. An R&D is ongoing to improve the cube size manufacturing precision.

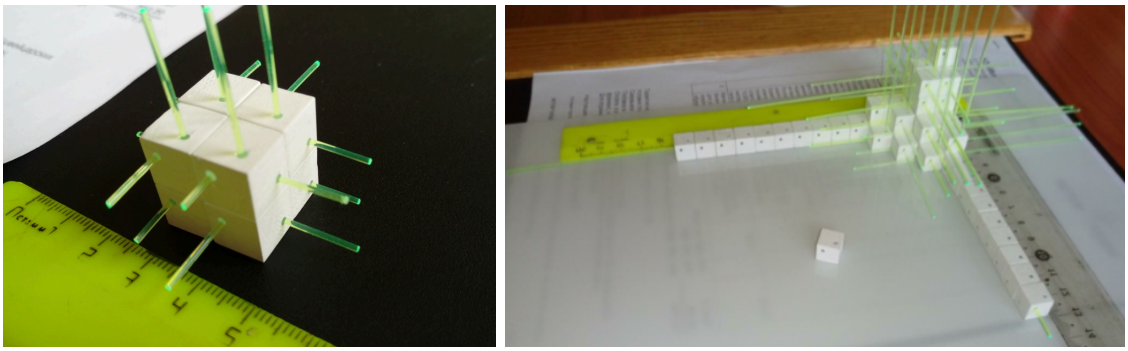

Figure 13: Picture of a small Super-FGD prototype . Several cubes of extruded plastic scintillator with three fibers inserted in the three holes are assembled. The size of each cube is $1 \times 1 \times 1$ cm^3.

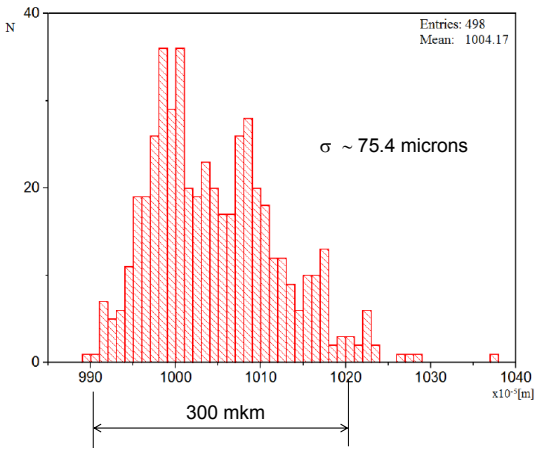

Figure 14: Measured dimensions of 166 scintillator cubes. Three sides are measured and plotted together. The distance between the two vertical lines corresponds to 300 μm.

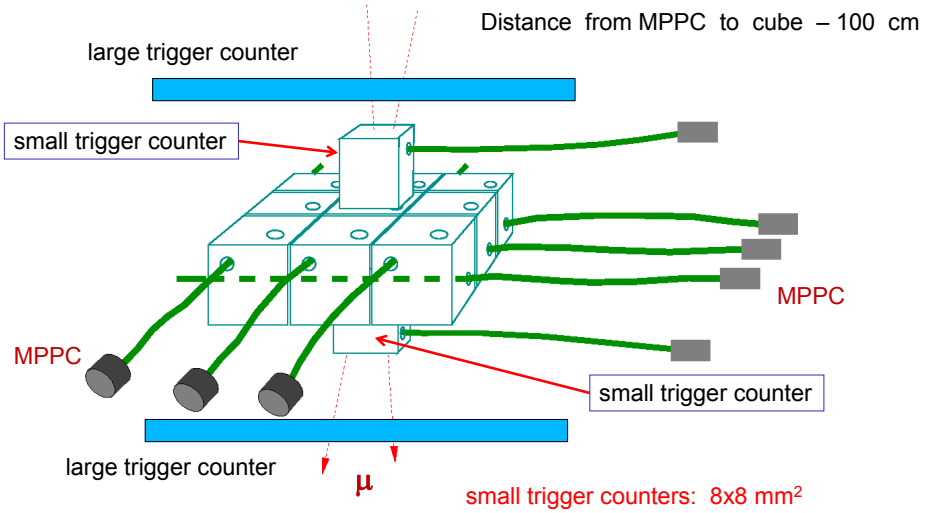

Figure 15: Setup of light yield measurement with cosmic rays

The light yield and timing resolution were measured with cosmic rays. Figure 15 shows a schematic view of the measurement setup. Scintillator cubes were read out via wavelength shifting fibers and Multi Pixel Photon Counters (MPPCs). The length of fiber was 1.3 m, with a distance between scintillator and MPPC of 1 m. The measured light yield is shown in Fig. 16. On average, the light yield was 50-60 photoelectrons at 1 m from MPPC. The timing resolution is found to be 0.91 ns RMS for 1 fiber readout and 0.63 ns RMS in the case the signal from two fibers is used.

A test beam experiment at CERN has been carried out in October 2017 to evaluate the performance in more detail. A small detector with 5×5×5 cubes has been assembled as shown in Fig. 17. More information on the performance of cubes will be known with the analysis of test beam data.

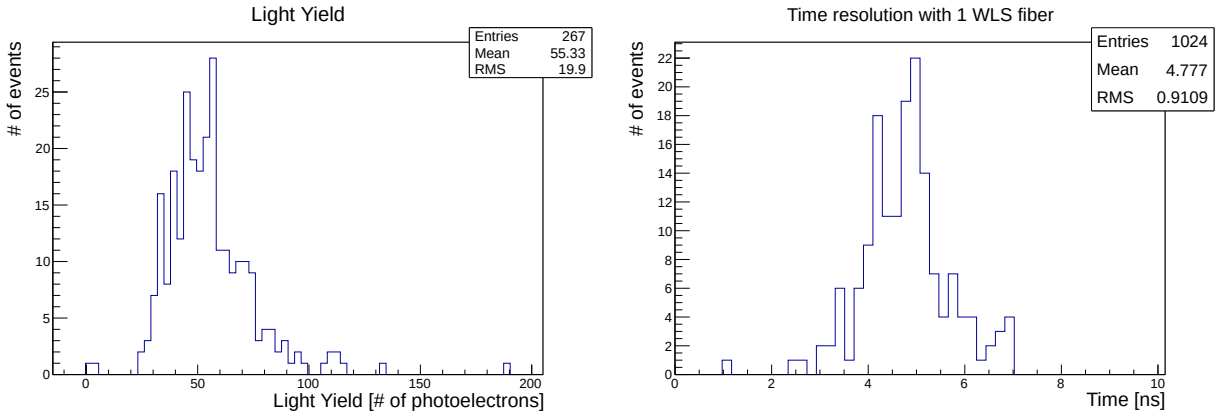

Figure 16: Measured light yield (left) and timing resolution (right) of $1\times1\times1$ cm^3 scintillator cubes.

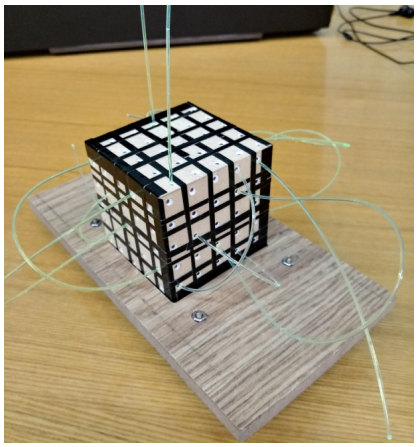

Figure 17: Small detector with $5\times5\times5$ cubes for a beam test at CERN.

5.2.2 FGD-like scintillator bar detector

Like the FGD in the current ND280, a detector consisting of plastic scintillator bars is one of the considered options. In order to match the acceptance of the horizontal TPCs for the large angle tracks, the bars will be arranged in x-z orientation (Fig. 18), rather than x-y in the current FGD.

Table 4: Main parameters of the FGD-like detector of the size of $1.8\times0.6\times2.0$ m^3, assuming 1×1 cm^2 bars.

Parameter	# of bars	# of channels	Total fiber length
	11,400	11,400	22 km

The plastic scintillator bars will be produced by extrusion. Figure 19 shows the cross section of a scintillator bar used for the FGD of T2K ND280 [26]. It is made of polystyrene doped with PPO (1%) and POPOP (0.03%). A reflective coating consisting of polystyrene doped with TiO_2 is co-extruded. The production procedure is established in Fermilab [27]. The Fermilab facility produced scintillator bars for neutrino detectors, such as K2K SciBar, MINERvA, T2K INGRID/P0D/ECAL, and WAGASCI, and the production of 1 cm^2 size bars is well established.

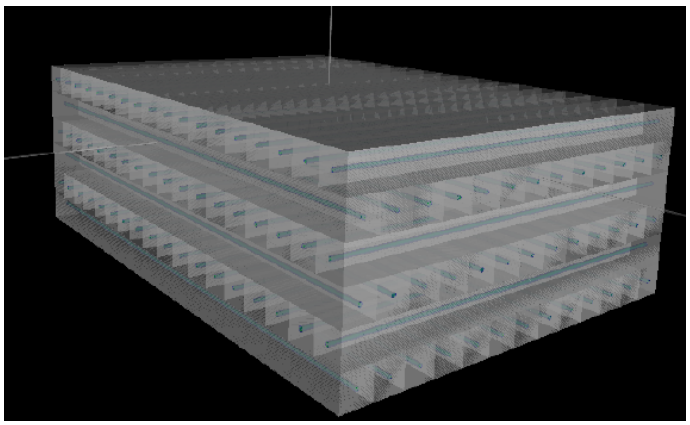

Figure 18: Schematic of FGD-like structure.

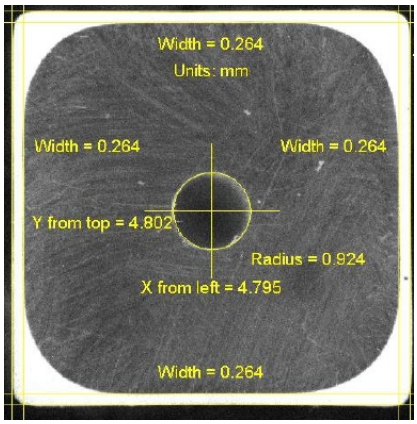

Figure 19: Cross section of a scintillator bar used for the FGD of T2K ND280 [26].

Table 4 summarizes the parameters of a FGD-like detector with 1×1 cm^2 bars. The number of channels and amount of material are similar to the sum of existing two FGDs. The assembly and mechanical structure for the FGD-like detector are expected to be similar or simpler to those of the Super-FGD. Thus, a large part of mechanical study for the Super-FGD is considered to be applicable also for FGD-like detector design.

5.3 Wavelength shifting fiber

Wavelength shifting (WLS) fibers are commonly used to collect light from large area of scintillators. Specifically, Kuraray Y11(200) fiber is widely used in recent neutrino detectors, and its performance is well established as a standard. One end of each fiber can be mirrored to increase the photon yield, if necessary.

5.4 Multi-Pixel Photon Counter (MPPC)

As a photosensor for scintillation light detection, we plan to use Multi-Pixel Photon Counter (MPPC) produced by Hamamatsu Photonics. MPPCs have been successfully used very stably in all of scintillator-based detectors in the current ND280. For the upgraded detector, we plan to utilize the latest version of

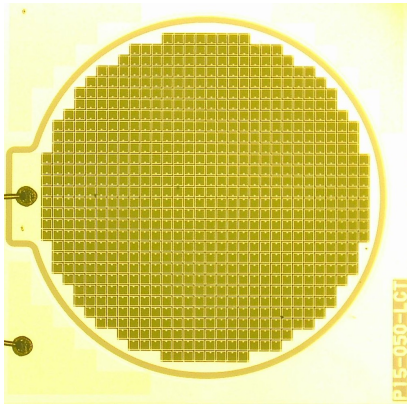

Figure 20: Microscopic photo of one MPPC used for INGRID Water Module and the T59 WAGASCI detector. The size of a pixel is 50×50 μm^2 and the diameter of sensitive area is 1.5 mm.

MPPCs, incorporating recent improvements of performance. Figure 20 shows a picture of recent MPPC developed with Hamamatsu for the WAGASCI detector, employing a round sensitive area of 1.5 mm diameter.

Figure 21 shows the comparison of measured performance of three generations of MPPCs [28]. S10362 is the version used for the current ND280. S13081 is the latest version of the MPPC (now available as S13360). The new MPPC has significantly less dark noise rate and cross talk probability, allowing a lower threshold. Thanks to an order of magnitude lower dark noise rate, the new MPPC can be operated with higher over-voltage than those for the current ND280, resulting in higher gain and higher PDE (photo-detection efficiency).

With the existing ND280 detectors, we have experience of production, test, and characterization of a large number of MPPCs [29, 30, 31].

5.5 Readout electronics

There are several candidates for the readout electronics. The current FGD uses electronics based on AFTER ASIC [20], while other detectors use Trip-t based electronics [32]. For a test experiment T59, a readout system based on SPIROC2 chip [33] has been developed. A similar chip, CITIROC, is used for the Baby-MIND detector [34] (Fig. 22). A similar design to those electronics is expected to satisfy the requirements for SD. Design work based on these front-end ASIC technologies is expected to start soon. The design will be fixed considering the specifications, e.g. the timing resolution and dead time, and available resources.

5.6 Mechanics and integration

The mechanics and integration will be a challenge especially for the Super-FGD structure, while those for the FGD-like structure will be somewhat simpler with much overlap of issues. Thus, the current R&D is focused on the mechanical issues with Super-FGD design.

The Super-FGD consists of O(2M) plastic scintillator cubes. In order to avoid possible damages to

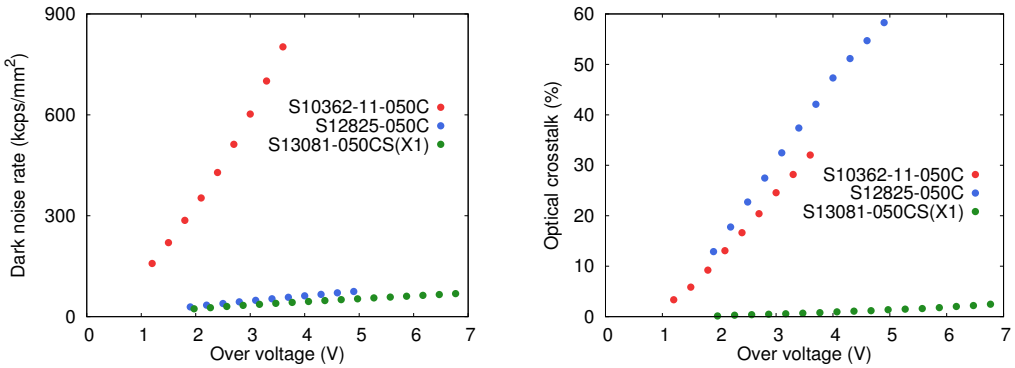

(a) Dark noise rate

(b) Optical crosstalk

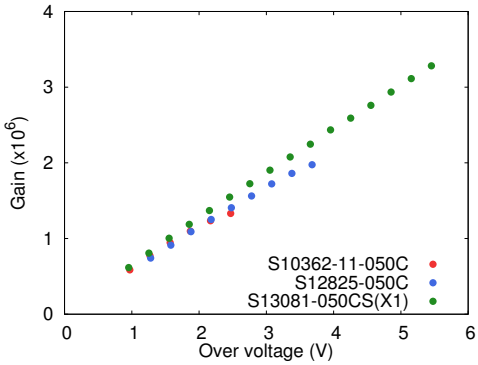

(c) Gain

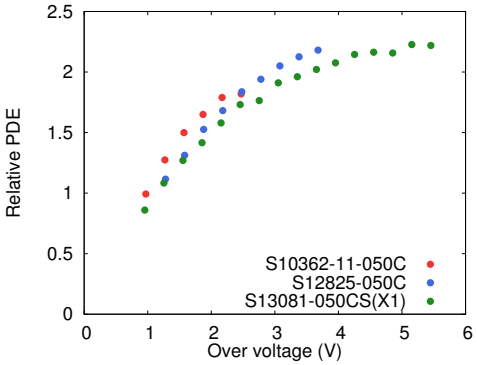

(d) Relative PDE

Figure 21: Measured performance of MPPCs. S10362 is the version used for the current ND280. S13081 is the same MPPC structure as those used for the INGRID water module. S12825 is an intermediate version without cross talk suppression. [28]

the coating, we do not plan to glue the cubes to each other. Furthermore, given the very large number of cubes, gluing all of them would increase the assembly time by a non-negligible amount of time. A box that contains all the cubes is needed. It must be strong enough to keep the cubes in place, and support about 2 tons. It must also resist to the mechanical stresses during the shipment or due to earthquakes.

The current design of the box is shown in Fig. 23. Each panel consists of a 30 mm thick AIREX layer sandwiched between two 2 mm thick carbon-fiber skins. From preliminary Finite Element Analysis (FEA) simulation studies we expect a maximum deformation of 1.7 mm in the middle of the bottom panel. The carbon-fiber skins ensure enough rigidity against the mechanical stresses. The AIREX material has very low density (about 60 kg/m^2), is similar to honeycomb but homogeneous, and provides good rigidity combined with a very low material budget. Inside the box a soft foam material will be used to fill the remaining empty space and keep the cubes in place.

The readout system will be placed outside the box. In all the panels, except the bottom one that support the structure, many holes will be done in order to let the WLS fibers exit the box and bring the light to the corresponding MPPC. In order to allow an easier assembly of the detector, the carbon-fiber box will be open on the three sides and closed once all the cubes are in place. Several screws will be used

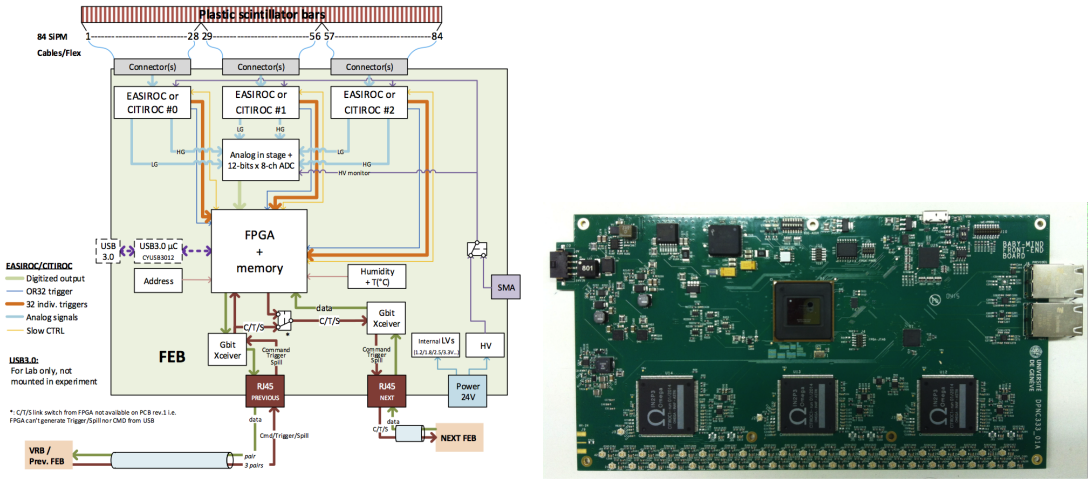

Figure 22: Schematics (left) and picture (left) of the frontend board for Baby-MIND detector.

along the vertical edges to provide enough strength.

Simulation studies and a prototype will be made to optimize the design.

6 Time-of-Flight Detector

6.1 TOF goals and configuration

The primary goal of the time-of-flight (TOF) system is to precisely measure the crossing time of charged particles. Combined with a timing measurement in the SD, this allows the determination of their direction and to separate the incoming background from the products of neutrino interactions in the inner part of the detector. An additional goal is to improve the particle identification.

The TOF will cover the outer side of the volume where the SD and the HA-TPC will be installed. The upstream and downstream TOF layers will be installed inside the basket, while the top, bottom and side layers will be mounted on the P0D ECAL, the electromagnetic calorimeter covering high scattering angles.

The required timing resolution is around 0.5–0.8 ns to determine the direction of charged particles, while particle identification might benefit from a better timing resolution.

In the following subsections we are going to describe two alternative detector technologies that are being considered for the TOF system.

6.2 TOF based on cast plastic scintillator counters

A TOF detector based on the concept of bulk plastic scintillator bars read out directly by large-area silicon photomultiplier (SiPM) arrays provides as an attractive option for the TOF detector of the ND280 upgrade. This novel design was developed by the U. Geneva group in the context of the Fast Advanced Scintillator Timing (FAST) action of the European COST programme. Such a detector has applications in particle physics experiments which need to cover a large surface with a timing resolution below 100 ps

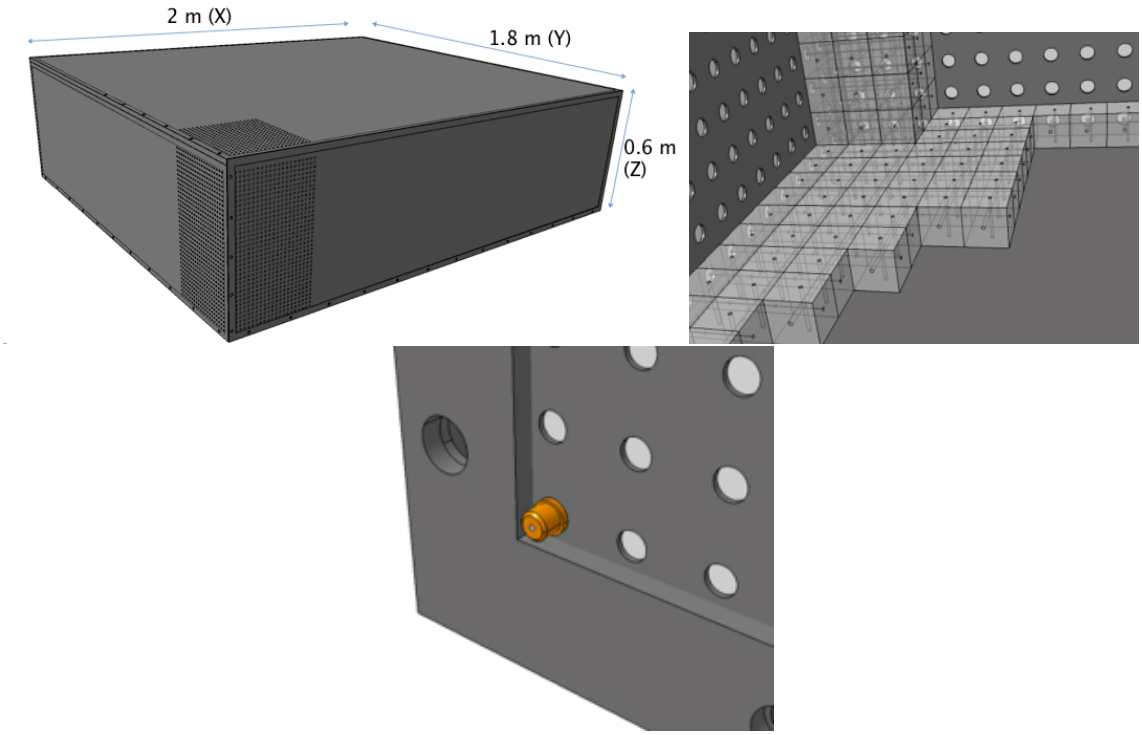

Figure 23: Top Left: the carbon-fiber based box is shown. The dimensions are 1.8 (width) $\times$ 0.6 (height) $\times$ 2 (length) m^3. Top right: the cubes assembled inside the box are shown. Holes are made to let the WLS fibers exit the box. Bottom: the corner of the box is shown with a MPPC inserted in one of the holes. On the edge larger diameter holes are made for closing the box with screws.

even in the presence of a magnetic field.

As a first test, a 300 cm $\times$ 2.5 cm $\times$ 11 cm counter read out on both sides by photomultiplier tubes (PMTs) was exposed to a test beam at CERN to study its light yield and timing characteristics as a function of position and angle of incidence [35]. This permitted to validate our model of light propagation, attenuation and detection and understand in detail the factors affecting the time resolution, such as the bar length and thickness, the type and coverage of the photosensor, and the signal shaping and analysis using waveform digitisers.

The replacement of PMTs by modern SiPM sensors offers several advantages: magnetic field tolerance, a much smaller volume and footprint allowing a compact design for bars without light guides, and an increased sensitivity to the part of the light spectrum (towards the green) which is least attenuated inside the bar. While these factors are expected to lead to a better timing performance, until recently the cost of SiPMs per unit area has typically been at least a factor $2-3$ higher than that of traditional PMTs. However, competition amongst a handful of manufacturers, increase in demand and improvements in processing are all leading to the availability of cheaper SiPMs, which makes the cost of such devices competitive or even advantageous even for a large area coverage.

One issue when using large-area SiPMs for timing is that the rise time of a signal increases with the sensor capacitance, which is proportional to the total area. The solution is to arrange relatively small

sensors (6×6 mm^2 was found to be optimal) in an array and read and amplify the individual signals from each sensor separately with a dedicated ASIC such as MUSIC [36] before summing them. This arrangement yielded very promising results in test-beam measurement with a first module prototype, where a time resolution around 80 ps was found all along a 1.5 m bar [37].

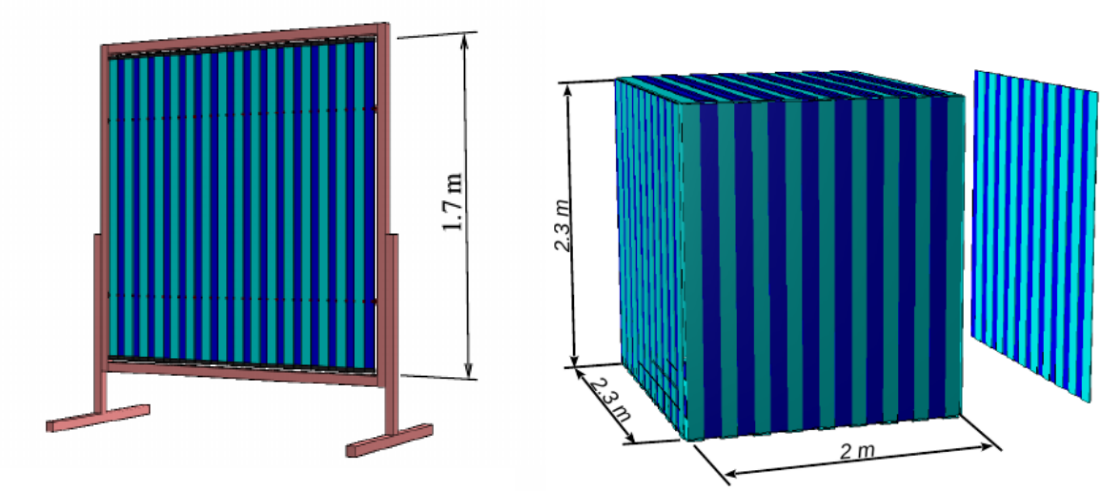

Figure 24: Schematic view of the timing detector prototype to be built and tested in 2018 (left) and the TOF detector for the ND280/T2K upgrade (right).

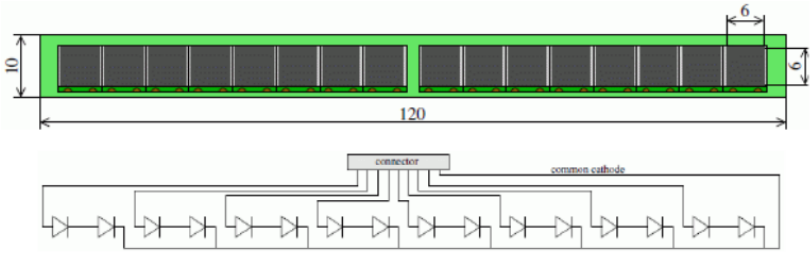

Figure 25: Arrangement for the light collection at each end of the bar for the cast scintillator TOF, with 16 large-area SiPMs connected in parallel for pairs connected in series, applied directly to the bar surface.

A prototype array comprising 32 bars of type EJ-200 of dimension 168 cm×6 cm×1 cm (depicted in Fig. 24, left) is in development and will be built in Spring 2018. The bars can be arranged as a single array or as two perpendicular arrays of 16 bars each. This prototype will allow to study the interaction of adjacent bars and determine the final efficiency and time performance in the overlapping regions for various angles of incidence. We will also test various options for the synchronisation procedure: using overlaps between bars, using a separate TOF counter placed upstream, and using a system of light pulse delivery with optical fibres.

The prototype will be installed at the end of 2018 as a part of the test-beam setups for ND280 upgrade (see Section 7). Placed in front of the scintillator detector and the high-angle TPC, it will serve as a trigger array and provide time-of-flight information to tag the different particle species inside the beam. It will

also play the same role for the test beam of the high-pressure TPC [38].

The final detector, expected to provide a time resolution of 100 ps, will be made of bars of type EJ-200 with dimension 230 cm×12 cm×1 cm. It will comprise three modules of 20 bars in the xy and four modules of 11 bars in the xz and yz planes for a total of 208 bars, as schematically depicted in Fig. 24 (right). For each bar, the light will be read out on both sides by an array of 16 6 mm×6 mm SiPMs connected in parallel for pairs connected in series, as depicted in Fig. 25.

6.3 TOF counters with WLS fiber readout

In this subsection we will describe a TOF detector based on wavelength-shifting (WLS) fiber readout.

Scintillator bars with WLS fibers and opto-electronic readout are considered as an established technology for massive neutrino tracking calorimeters in long-baseline neutrino oscillation experiments. The parameters for the conceptual design of TOF counters are determined by the technology developed and applied in the ND280 scintillator detectors [39] as well as by the cost considerations. Manufacturing extruded scintillators is a well proven technology: 7 mm thick extruded scintillator bars or slabs produced a high light yield and demonstrated good stability over years of the T2K operation.

Y11 Kuraray WLS fibers are used for the readout. The fiber readout provides high response uniformity over the scintillator volume. The length of the fibers and counters is limited to 2.6–2.8 m by the available space. A slow re-emitting decay time of Y11 fibers (∼12 ns) is compensated by the high light yield achieved for WLS fibers. The spacing between the fibers is proposed to be 5 cm. The density of the fiber readout (number of the channels) in this case looks like the optimum between the desirable performance and acceptable cost of the detector. The studies of the fiber density were performed in many beam tests of scintillator counters with WLS fiber readout.

R&D work was done to find the optimum readout configuration of 3 m long scintillator detectors read out with long WLS fibers and Hamamatsu MPPC photodiodes. Results of the timing measurements are presented in the next section.

6.3.1 Cosmic tests of 3 m long TOF prototypes with WLS readout

A few scintillator samples were made from 7-mm thick extruded scintillator slabs with grooves spaced at 5 cm. The width of the samples was 5, 10, 15 and 20 cm. The 5-cm wide samples have a single groove. The length of the samples varied from 15 to 120 cm. The length of the WLS fibers was fixed to 3 m. Y11 Kuraray multi-clad fiber of 1 mm diameter are viewed from both ends by Hamamatsu MPPC SiPMs of two types, 1×1 and 3×3 mm^2 size. The signals from MPPCs were amplified by a custom-made preamp with gain of 20, then sent to the 5 GHz sampling digitizer CAEN DT5742. Cosmic trigger is arranged with 2 cm wide scintillator counter which was placed across the tested samples.

Fig. 26 shows the two tested configurations with four 5-cm wide tiles and two 10-cm wide tiles. In both sets 4 fibers are used. The fibers are read out either individually by $1 \times 1 mm^2$ MPPCs (S12571-025C) or by a single 3×3 mm^2 MPPC (S12572-050C) at each side combining 4 fibers per the MPPC. Smaller MPPCs are connected in parallel at each side so that only two front-end electronic channels are used in

both readout schemes.

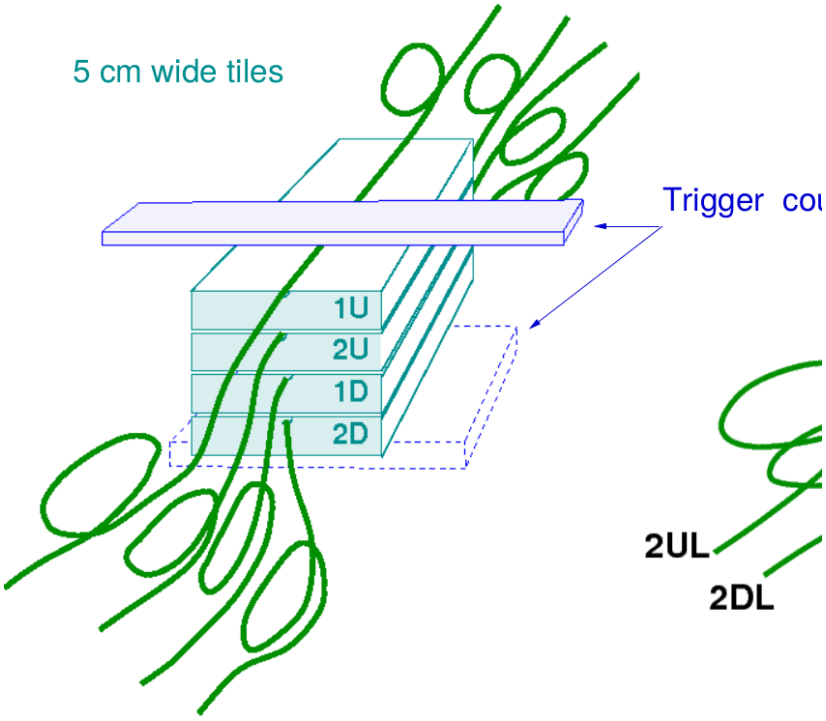

Figure 26: TOF prototype detectors based on WLS readout. Two tested sets of tiles are shown: 5-cm wide (left) and 10-cm wide (right). The WLS fiber length is 3 m.

882

883 The time resolution of the counters was measured as follows. The time of an individual signal was
884 obtained with the constant fraction method. The maximum amplitude of a digitized signal waveform was
885 measured, then the time mark is defined as the time where the signal front reaches the 0.1 fraction of the
886 maximum amplitude. The combination T=$(T_L - T_R)/2$ was plotted, where T_L and T_R are the timing
887 from both sides. The difference of times are used to subtract the contribution in time fluctuations from
888 the digitizer uncertainty and the jitter of trigger signals.

889 The main results obtained in the cosmic tests are reported below.

890 • We observed no difference in the time resolution if we merge WLS fiber light on a single large
891 $3 \times 3\ mm^2$ MPPC or sum pulses from small $1 \times 1 mm^2$ MPPCs connected in parallel.

892 • The width of the counters does not affect the resolution at the same spacing between WLS fibers,
893 as shown in Table 5.

894 • The time resolution was measured for a few layers of 5-cm wide counters with large MPPCs and
895 small MPPCs connected in parallel. The obtained results are:

896 σ_t=800–870 ps for a single layer;

897 σ_t=600–630 ps for two layers;

898 σ_t=500–530 ps for three layers;

899 σ_t=450 ps for four layers.

Table 5: Parameters of 7-mm thick counters with 3 m long WLS fibers. The spacing between fibers is 5 cm in all counters.

Width, cm	Number of fibers	Timing σ_t ns	Light yield p.e./MIP
5	1	0.85	80.0
10	2	0.80	88.3
15	3	0.87	78.6
20	4	0.86	78.1

6.3.2 Proposed concept for TOF counters with WLS fiber readout

The TOF module consists of two combined scintillator slabs of $0.7 \times 20 \times 270$ cm^3 size with 4 WLS Kuraray Y11 fibers of 1 mm diameter in each slab. 8 WLS fibers spaced at 5 cm are bundled within a scintillator slab into an optical connector at each side. The connector is mounted directly in the scintillator. The fibers are read out by a single 3×3 mm^2 MPPC. The expected time resolution of the module σ_t is 630–650 ps, and the light yield is 160–170 p.e./MIP. The conception of the module is shown in Fig. 27.

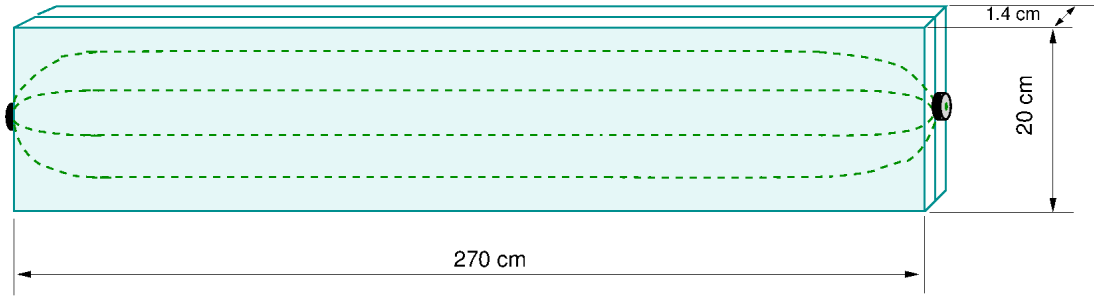

Figure 27: Concept sketch of the TOF module.

The TOF system will consists of 152 TOF modules with 304 readout channels. The total weight of scintillator counters is about 1300 kg.

7 Test Beam

7.1 Test beam goals: detector characterization

The ND280 Upgrade will be based on innovative detector technologies. We plan to conduct detailed characterization of the response of detector prototypes in order to validate the technical solutions adopted for the detector design and construction. This concerns in particular the TPC and the scintillator detector.

The TPC prototype will consists of a prototype of the TPC field cage hosting one or two Micromegas detector on its end plate. The overall dimensions are approximately 1m $\times$ 1m $\times$ 0.6 m, for 90 cm drift

length and a tracking length of approximately 35 cm (70 cm in the case of two Micromegas). The main goals of the beam test of this prototype are:

- System test, including operation at the nominal electrical field configuration, gas drift properties, gas purity etc
- Study of the uniformity of the electrical field and the performance of the field cage
- Study of the Pad Response Function and its uniformity across the Micromegas sensitive surface
- Study of the dE/dx resolution
- Optimization of the read-out electronics configuration and in particular the peaking time and the gain settings.

The TPC setup will consist also of several scintillator as hodoscopes and TOF, and for triggering on cosmic ray.

With a beam of TOF-selected pions, protons, electrons and muons in the 0.5-2 GeV range, we plan to expose the TPC prototype to tracks at different drift lengths and incident angles. Further data-taking with cosmic rays will complement this dataset.

The scintillator detector prototype will consist in a medium size detector, built with several thousands scintillator cubes. The main goals of this test are:

- Study of the detector response: light yield, timing properties, cross-talk.
- Study of the detector response with different charged particles

7.2 Test beam facility

Considering the peak energy (600 MeV) of the T2K off-axis beam, most of the charged particle to be reconstructed have momenta below 1 GeV. The PS T9 or T10 beam lines are the most interesting for this test. A request to the PS-SPS coordinators has been done for two beam periods (each for two weeks) in 2018 to test the TPC and the scintillator detector prototype.

For the TPC we foresee to use a low intensity beam (DAQ event rate is limited to 50 Hz) with approximately 100 particles per spill. We need beam instrumentation to select the particle type with Cherenkov detectors and hodoscopes to provide the trigger for the TPC DAQ. For the TPC we will use premixed bottles with the T2K TPC gas mixture (Ar-CF4-isobutane, 95-3-2%).

Concerning the magnetic field, we will be able to operate the TPC without it, relying on the beam instrumentation for PID (the beam below 1 GeV consists of pion, muon, electrons), and on the beam collimators to define the momentum bite. However, by carefully designing the TPC prototype and limiting its overall dimensions, it will be possible to insert it in the HARP magnet. This will open the possibility to continue the prototype tests after 2018 with cosmic rays, provided we can operate the HARP magnet with a low magnetic field (0.2 T).

The LS2 period without beam will not allow to expose the final detectors to a charged particle beam for a characterization of the detector response and precise calibration in 2020. However, we will consider the possibility to do this beam test in other European laboratories like DESY or PSI.

8 Interface with Existing ND280 DAQ and Online and Offline Software

The ND280 data acquisition systems and online and offline software were designed and built specifically for the detector, and have been running smoothly since first data in 2009, with ongoing debugging and proactive maintenance work resulting in no substantial data loss or data processing issues caused by problems with these systems.

The ND280 subdetectors belong to two groups: those with readouts based on the Trip-t ASIC (originally designed at Fermilab), which were designed and built in the UK; and the FGD and TPC, with their custom AFTER ASIC-based readouts which were primarily developed in France. The outputs from these front-end systems are then collected by a back-end DAQ system which is made up of readout merger modules (RMMs), a master clock module (MCMs), slave clock modules (SCM), and cosmic trigger modules (CTMs), all of which are built on a common hardware platform developed at RAL in the UK. This system also allows for the triggering of the entire detector suite when certain internal and external conditions are met.

The software interface with the DAQ electronics is based on MIDAS, with additional custom features that have been built upon this to help improve the efficiency and reliability of the use of the DAQ output files, with the offline software being able to read the raw data files as if they were native offline files. This is done by passing on, directly to the offline software, the files which define how data are encoded in the MIDAS online systems. This online-offline mechanism was written as a UK-led effort within the ND280 Software Group.

For the offline software, the format for MC simulation information mirrors the form that the real data appears within it; this allows real data and MC to be treated in identical ways, as appropriate, as they are passed through the calibration, reconstruction and analysis stages of the software framework. The software suite was built through the collective effort of software group members from across the collaboration, whilst the group has had a significant amount of UK effort in its coordination and leadership, and continues to do so.

For any new detectors to be integrated successfully into this system, and to be accessible for seamless analysis use alongside the existing detectors, it is important that the relevant aspects of their design and construction are aligned with the schemes outlined above. This includes, in particular, the interfaces of the new detector readouts to the MCMs; the encoding of detector data into the binary form conveyed through MIDAS, and the formats used to define this encoding; the schema within which detector calibration and alignment are handled, and the framework for implementing reconstruction algorithms and producing analysis output. This was reported at the ND280 Upgrade workshops in the first half of 2017, and broad consensus was reached regarding the need for consistency in these designs between the existing and upgrade detector systems.

Members of the existing DAQ and Software groups are willing to advise and support those who will be designing and implementing these for the new detectors, and to request further resources to bolster this support, under the condition that this design consistency requirement is met. In addition to this, there are

many opportunities for the software and the infrastructure within which it is developed and deployed to be modernised compared to the early-2000's technologies on which they are currently based—and existing and new collaborating groups are welcome to help develop these further to meet the needs of the upgraded ND280 detector.

9 R & D for a High Pressure TPC

In the long term, the physics goals of T2K motivate a progression of reducing neutrino cross section uncertainties down to the 2% level, into the era of Hyper-K. As statistical errors decrease with time, the CP violation analysis will become systematics-limited (rather than statistics-limited, as is the case now), and therefore an improved treatment of the systematic uncertainties associated with the choice of theoretical model for the background processes is required. For example, the effects of charged current multi-nucleon, $\nu_\ell p, n \to \ell^- pp$ (CCMN), modelling uncertainties are an active area of study in both the theory and experimental communities. A second example is the effects of hadronic final state interactions (FSI), which can modify the multiplicity and kinematics of secondary particles created by neutrino-nucleus interactions. Both of these topics present a strong challenge to the long term goals of 2% systematic errors. The aim of the High Pressure TPC (HPTPC) is to provide high-resolution measurements of neutrino interactions to reduce cross-section uncertainties, such as those from CCMN and FSI. The R&D goals for the HPTPC work package enjoy strong synergies with the other work packages in this proposal.

We will develop the design for an HPTPC near detector, with the purpose of identifying and reconstructing the final state particles that emerge from the neutrino interaction vertex with extremely low momentum thresholds. This should be able to mitigate the neutrino interaction cross-section uncertainties, particularly for CCMN, by improving the ability to distinguish between different final state topologies. This is accomplished through lowered momentum thresholds for final state particle detection, and 4π coverage of the fully-active interaction volume with no dead layers. Mitigating the uncertainties from FSI modelling can be done by making precise measurements with a range of nuclear targets, which is possible by changing the TPC gas. To lower the momentum threshold, increased readout resolution is desirable. Changing target gases presents a different set of challenges due to the different drift velocities, diffusion parameters, and gas gains that will be experienced with different target gases. Recent progress with micropattern gas detectors, driven by development for this T2K upgrade, as well as LHC, and ILC has made high-resolution readout of TPCs possible at a large scale. We seek to develop hybrid readout systems employing high resolution micro pattern detectors in conjunction with high resolution optical readout systems. The optical readout system design draws on the R&D efforts to build a 1 m^3 optical HPTPC prototype for use in a test beam; the testbeam request has been submitted to the CERN SPSC, as CERN-SPSC-2017-030 and SPSC-P-355, within the context of EOI-015. The combination of optical readout with direct charge readout can create a detector system that achieves the resolution specifications while at the same time addressing the challenges of using multiple target gases.

The $1m^3$ prototype is an intermediate stage on the road toward the full neutrino detector; we envision to install a 20 m^3 HPTPC detector on the neutrino beam in the JPARC NM pit. Thus far, we have

developed the simulation of the prototype detector and extrapolated to a neutrino detector simulation, studied the gas composition and readout pitch, and used T2K analysis tools to study the impact of an HPTPC on the near detector cross section constraints. We have demonstrated that tracking with 50 MeV/c threshold for protons is viable if the pitch is at the mm scale; this is to be compared with the proton thresholds of 200 MeV/c in liquid argon and 1100 MeV/c in water Cherenkov detectors. The increase in beam power expected from the Main Ring upgrade means that a high-pressure gas detector can accumulate $\sim 10^4$ events per year for a TPC target at 10 bar pressure.

In terms of physics studies, we are developing new analysis ideas to utilise the high quality data foreseen from HPTPC neutrino detector. New event selection criteria based on emerging ideas, such as the momentum imbalance in the plane transverse to the neutrino direction, that take advantage of the extraordinarily low momentum detection thresholds of the gas detector are being studied and applied to neutrino oscillation analyses. Using such HPTPC event samples as a constraint on the cross section parameter uncertainties in the current T2K near detector analysis, we have demonstrated that the HPTPC can improve purity of exclusive final state selections and hence reduce the uncertainties on the normalization uncertainty of CCMN and the target Fermi momentum by more than a factor of 2. An optimal HPTPC analysis, including the high-resolution final state lepton and hadron information and associated correlations, will provide more powerful constraints and is under development.

We note that the HPTPC and ND280 detector provide highly complementary data sets. While the HPTPC targets multi-nucleon final states down to low momentum, the statistics are relatively low; the the ND280 detector provides relatively high statistics samples and the upgraded tracker will provide a new window into neutrino-nucleus kinematics. Both detectors can provide good, and complementary performance on intrinsic ν_e background constraints and neutrino energy reconstruction, with different focus. The strength of the HPTPC is not just the low momentum threshold, but the possibility of using multiple target gases to constrain the nuclear model.

On the timescales of this proposal we plan to take forward the existing R&D phase of the programme from a simulation and validation effort into prototyping and feasibility studies, specifically with respect to high-resolution HPTPC readout since this will be the cost-driver for this detector. Our baseline readout concept is a modification of the existing TPC electronics to use strip rather than pad readout, with 1 mm pitch, and we will study using ancillary optical sensors to mitigate the reconstruction degeneracies of strips. The R&D goals for this period include: (1) a working charge readout plane prototype, using Micromegas and TPC pad readout electronics; (2) DAQ software to use the TPC readout back-end for charge strip readout; (3) software interface of the charge readout data format to existing TREx reconstruction package; (4) deployment of the prototype charge readout plane and electronics in the HPTPC prototype; (5) data taking in pad vs. strip mode to study final state particle threshold and track counting; (6) measurement of the reconstruction degeneracy, and impact on efficiency/purity, from strip vs. pad readout for cost optimization. The detector design goals include a full simulation of the HPTPC neutrino detector, with related subsystems, and development of a mock-data analysis that can take advantage of the high multiplicity data that an HPTPC can provide.

These goals benefit from strong synergies with the short term developments for the ND280 HA-TPCs,

namely the gas system design work, the Micromegas readout development, and the testbeam work. Developments for the HPTPC will leverage the expertise developed during the HA-TPC work.

10 Expected performances

The performance of the ND280 upgraded detector has been evaluated with simulations. The neutrino interactions were simulated with the GENIE software [40], while the geometry of the upgraded ND280 detector was simulated using GEANT4 [41]. The prediction of the T2K neutrino beam has been obtained with the JNUBEAM simulation [42], used for the official ND280 analyses. The beam is simulated both in neutrino enhanced (ν_μ dominated) and antineutrino enhanced ($\bar{\nu}_\mu$ dominated) modes.

The first goal was to optimize the design of the upgraded ND280 following the requirements described in Sec. 5. Also the current ND280 geometry was simulated using the same framework in order to directly compare the upgraded and current ND280 performances.

Different scintillator detectors were simulated, including the detector response, and the performances were directly compared (Sec. 10.1). The arrangement of the new sub-detectors inside ND280 was optimized by maximizing the efficiency to select Charged-Current neutrino interactions (Sec. 10.2). Finally in Sec. 10.3 the impact of the upgraded-like ND280 configuration on the constraint of the systematic uncertainties to neutrino oscillation is shown.

10.1 Scintillator Detector performance

The plastic scintillator technologies considered for the ND280 upgrade SD are presented in Sec. 5. Here the performance of the Super-FGD is compared with the FGD-XZ, where plastic scintillator bars are positioned along the X and Z directions in order to measure the tracks produced at high angles. Both detector responses are parametrized using either the measurement performed with test beams (from the FGD detector) or cosmic rays (Super-FGD). All the following effects are taken into account: the quenching of the light in the scintillator, the light collection efficiency in the WLS fiber, the light attenuation in the WLS fibers and the SiPM light-to-photoelectron efficiency. The Super-FGD is simulated as a parallelepiped of $1.9 \times 0.6 \times 1.9 \times \mathrm{m}^3$ size, built out of individual cubes of 1 cm side, each read out by three WLS fibers running along X, Y and Z. The simulated FGD-XZ detector has the same size as the Super-FGD, with plastic scintillator bars with a cross section of 1×1 cm^2.

The high granularity of the Super-FGD opens up superior possibility in term of pattern recognition and track reconstruction. This is illustrated by Fig. 28, showing an electron and a converted photon, and Fig. 29, showing two neutrino interactions.

The track reconstruction was implemented assuming a perfect pattern recognition but requiring the tracks to be separated by at least 1 cm, the size of the scintillator cubes and bars. A charged particle track is considered to be reconstructed if it has at least three hits in a 2D projection for Super-FGD. For FGD-XZ the requirement is to have 3 hits on a 2D-view, 4 layers along Y and $|\sin\theta| < 0.3$.

In Fig. 30 the reconstruction efficiency is shown for muons and protons produced by neutrino interactions for both Super-FGD and FGD-XZ. True muon tracks can be reconstructed with an efficiency higher

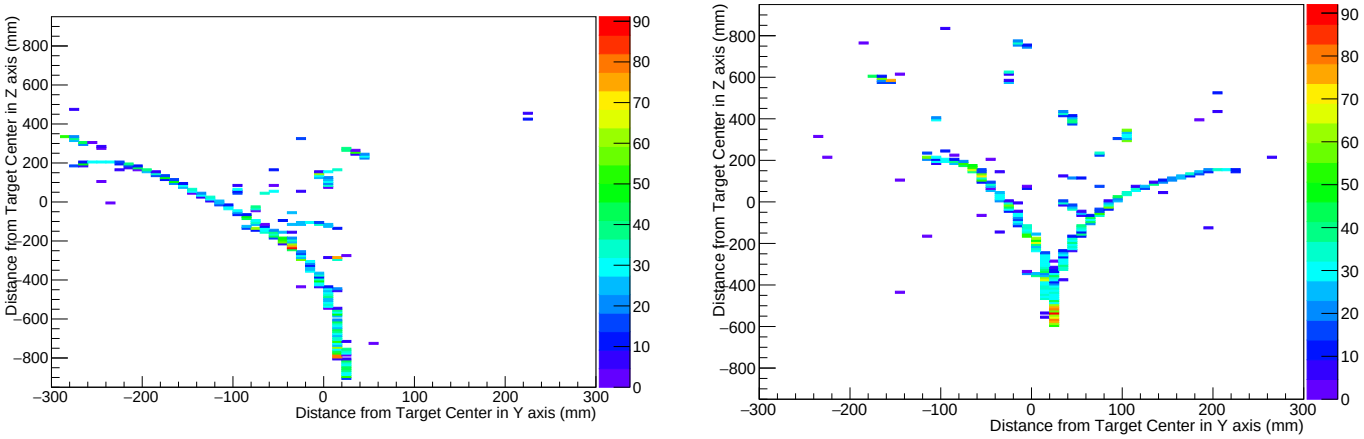

Figure 28: Simulated event displays of an electron track (left) and a converted photon (right) in the Super-FGD. The color shows the number of photo-electrons.

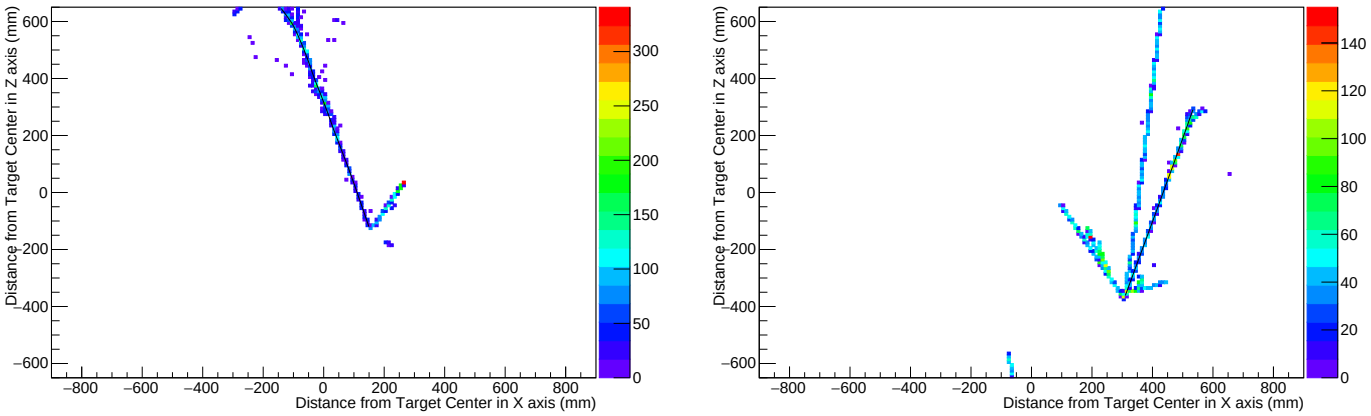

Figure 29: Simulated event displays of neutrino interactions in the Super-FGD. The color shows the number of photo-electrons.

than 90% for all the lepton angles in Super-FGD, while in FGD-XZ the efficiency is about 20% lower for $\sim 90°$ tracks. As shown, the weakness of a scintillator bars-based detector is the low efficiency for muons along the neutrino direction. Another advantage of the Super-FGD is the improved particle momentum threshold: protons down to approximately 300 MeV/c can be detected, against about 450 MeV/c with FGD-XZ.

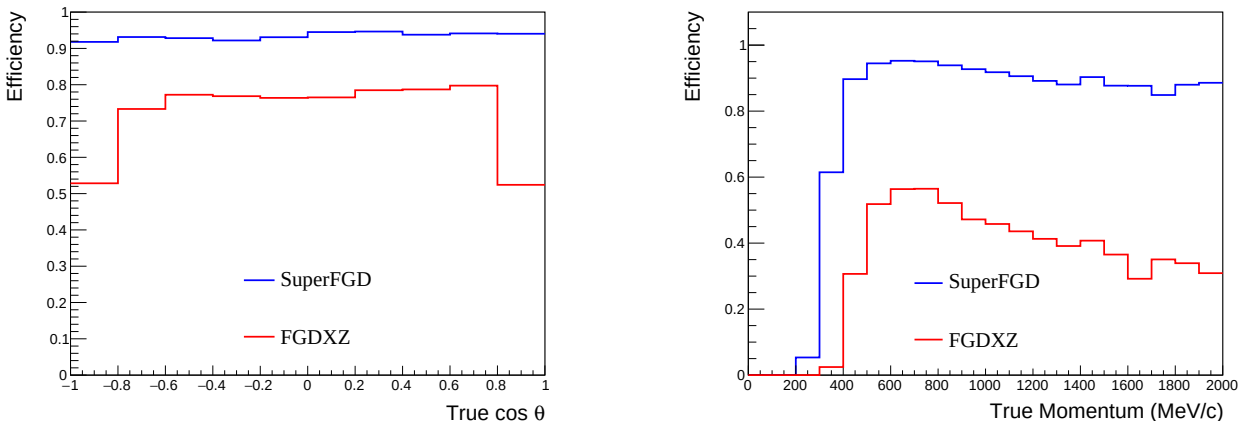

Figure 30: The reconstruction efficiencies are shown for the particles produced by GENIE-generated neutrino interactions. Left: muon reconstruction efficiency as a function of the true muon $\cos\theta$. Right: proton reconstruction efficiency as a function of the true proton momentum.

The Particle IDentification (PID) of protons and pions stopping in the target, based on the measured deposited ionization light, has been studied with both target detectors.

For Super-FGD the probability for a reconstructed muon to be misidentified as a proton is 8 %, while the probability for a proton to be misidentified as a muon is 17%. The PID performance of FGD-XZ does not differ significantly. A potential improvement could be obtained by applying different PID cuts at different reconstructed track lengths.

Studies of the $\gamma \to e^+e^-$ conversion in the target were performed. This is the main background to the measurement of ν_e cross section, given the difficulty to reconstruct both electron and positron tracks, in particular when the e^+ (e^-) stops before its track is separated from e^- (e^+). The γ PID was developed by tracking both e^+ and e^- produced by the γ conversion and, when reconstructed as a single-track event, by measuring the ionization light produced by e^+e^- in the scintillator, expected to be two times larger with respect to a single e^+ or e^-. A γ conversion with a single reconstructed track is identified as γ if the measured ionization light of the first segment is two times larger than the ionization light of the second segment. In Fig. 31 the SuperFGD distributions of the ratio between the dE/dx in the first and second segment of the track is shown for events not rejected by the tracking. The electron and $\gamma \to e^+e^-$ distributions are very well separated.

The expected probability to misidentify a $\gamma \to e^+e^-$ event as ν_e is about 19% in SuperFGD. The FGD-XZ detector has a worse capability to reject $\gamma \to e^+e^-$: the probability to misidentify it as a ν_e is about 33%. This means that the $\gamma \to e^+e^-$ background produced by ν_μ interactions occurring outside the

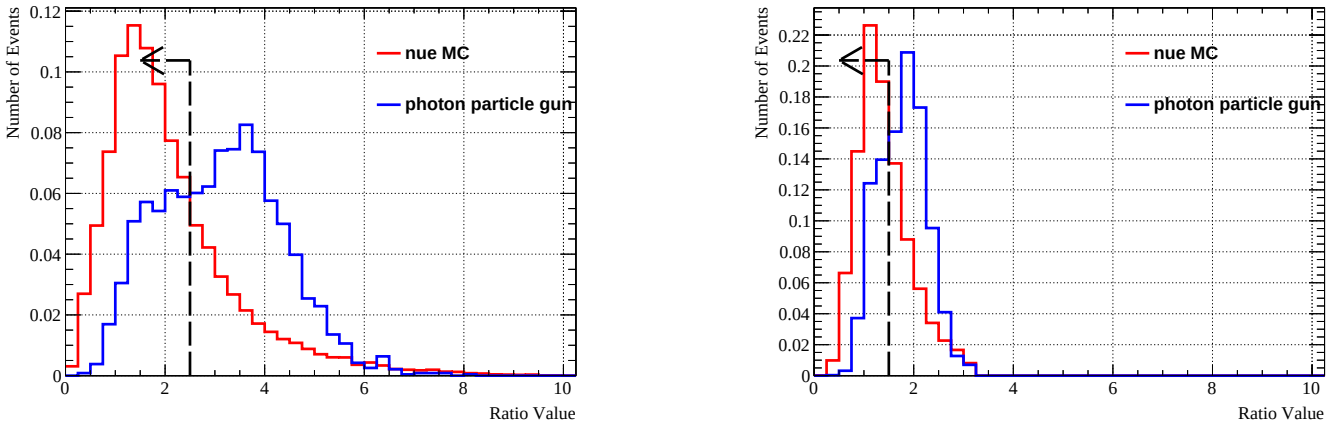

Figure 31: The distribution of the dE/dx ratio between the first and the second segment of the track in a Super-FGD detector (left) and FGD-XZ (right) is shown for both converted γ (blue) and electrons from ν_e interactions (red) with momenta between 200 and 600 MeV/c. In these figures only the events where only one track was reconstructed are shown.

fiducial volume is almost a factor 2 larger in FGD-XZ than SuperFGD. For both detectors the efficiency to select ν_e is about 77%. Further improvements could be achieved by studying the shape of the energy deposited around the reconstructed neutrino interaction vertex.

10.2 Neutrino event selection efficiencies

A selection of ν_μ and $\bar{\nu}_\mu$ candidate events was performed in order to evaluate the impact of the new HA-TPCs. A parametrized reconstruction was used for the TPCs. For instance, a track is reconstructed in one of the TPCs if the true track length on the readout projection is larger than 20 cm, consistent with the ND280 official reconstruction. The ECal performances of the official ND280 reconstruction were parametrized as a function of truth variables to be used in this study. The reconstruction and the PID in FGD1 and FGD2 were parametrized based on the ND280 official performance. For particles crossing the scintillator detector, the reconstruction efficiencies as a function of the true particle momentum and angle with respect to the neutrino direction, described in Sec. 10.1, were used. In this case the performance of the SuperFGD technology was considered. In order to reduce the CPU time and give the possibility to test many different configurations, the target detectors were simulated with uniform materials. The total neutrino target detector mass are 2.2 t for the current ND280 and 4.3 t for the upgrade. Only events with a neutrino interacting in one of the target detectors are selected.

Figure 32 shows the distribution of true muon momentum versus $\cos\theta$ for inclusive charged current events in the current ND280 and in the upgraded ND280. The improved and more uniform coverage of the high angle and backward region is evident. In Fig. 33 the selection efficiency for Charged-Current (CC) Inclusive ν_μ events in neutrino enhanced mode as a function of the muon angle with respect to the neutrino beam direction is shown. It is clear that the upgraded version of ND280 drastically improves

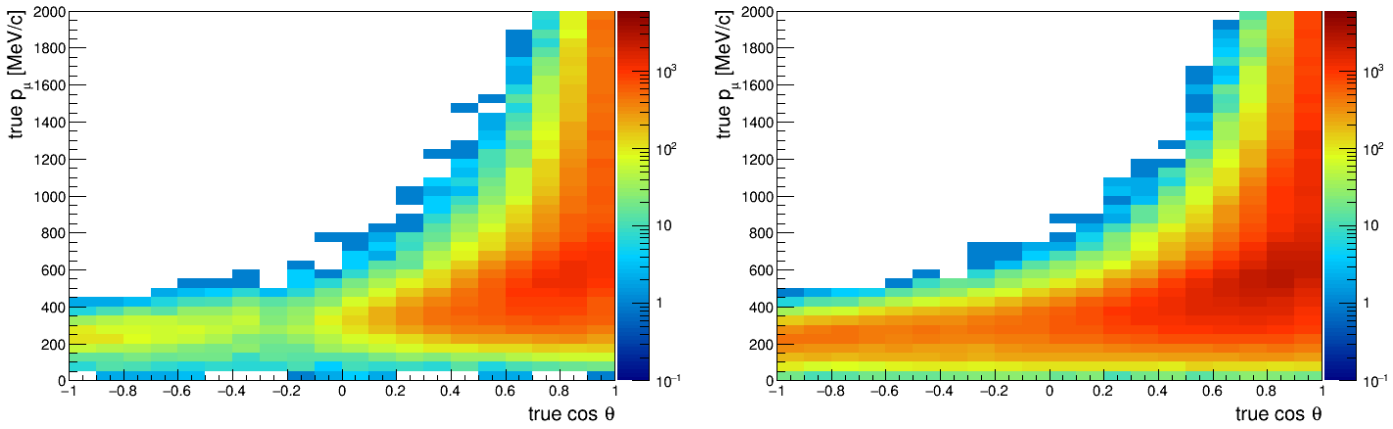

Figure 32: Distributions of the true muon momentum versus $\cos\theta$ for inclusive charged current events in the current ND280 (left) and in the upgraded ND280 (right).

the angular acceptance for muons produced at high angles, thanks to the new HA-TPCs, and backward, thanks to the TOF detector that allows to determine the track direction. Similar efficiencies are obtained for the CC-$\bar{\nu}_\mu$ antineutrino enhanced mode and neutrino enhanced mode.

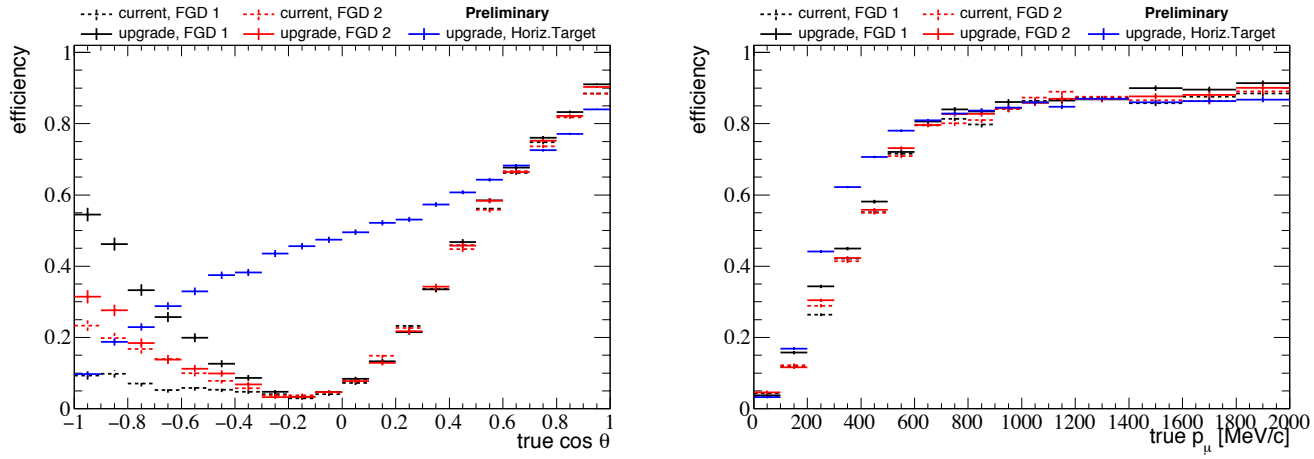

Figure 33: The ν_μ-CC event selection efficiency as a function of the true muon angle with respect to the z direction (left) and true muon momentum (right) is shown for both upgrade-like (solid line) and current-like (dashed line) ND280 configurations. The curves are shown for neutrino interactions in FGD1 (black), FGD2 (red) and horizontal target (blue) are shown.

The selected total numbers of CC events in each beam mode are shown in Table 6. Thanks to the larger target mass the upgrade ND280 configuration provides about twice the selected number of events compared to the current configuration.

Simulation studies were performed to estimate the Out-of-Fiducial-Volume (OOFV) background rejection, about 7% of the total number of selected events in the ND280 ν_μ official analyses. This background will become negligible in the upgraded ND280, well below 1%. Indeed the probability to reject an OOFV

Table 6: Predicted total number of selected events for each detector configuration and beam mode The prediction corresponds to 1×10^{21} POT. The out-of-FV is not included. The wrong-sign background is included only for $\bar{\nu}$ beam where it corresponds to a quite large fraction of events.

Selection	Current-like	Upgrade-like
ν_μ (ν beam)	93,401	194,654
$\bar{\nu}_\mu$ ($\bar{\nu}$ beam)	33,437	63,687
ν_μ ($\bar{\nu}$ beam)	17,998	33,773

Table 7: Predicted total number of selected ν_μ-CC events in neutrino enhanced mode for both ND280 upgrade-like and current-like configurations in each available neutrino target detector. The purity for each event topology is also shown. The prediction corresponds to 1×10^{21} POT. The out-of-FV and the wrong-sign backgrounds are not included because we expect this effect to be negligible.

		# of events	Purity (%)		
		($/10^{21}$ POT)	CC0π	CC1π	CC Other
current	FGD 1	50012	72.8	65.4	68.9
	FGD 2	48119	73.2	64.3	70.2
upgrade	FGD1	48332	74.6	65.0	69.6
	FGD2	45636	73.5	64.1	70.2
	SuperFGD	100686	73.9	72.9	70.9

event with the TOF detector was evaluated to be better than 95%.

The selected ν_μ-CC events separated according to the final state topology, i.e. CC0π (no charged pions in the final state), CC1π (1 charged pion) and CC-Other (all the other reaction modes), are shown in Table 7. The purity in the ND280 upgrade configuration is slightly improved.

Additional statistics and sensitivity could be gained by selecting CC-ν_μ interactions with a muon stopping in the target detector. Though this sample would be affected by a worse purity and the kinematic variables would be measured with a lower precision with respect to the sample with muons in the TPCs, we expect to add a potential 10-15% ν_μ-CC events, with an expected purity better than 80%, for physics measurements. In particular this sample would contain mainly low momentum muons, particularly powerful to constrain the nuclear recoil models, like 2p2h.

Another goal of the upgrade of ND280 is the measurement of the ν_e ($\bar{\nu}_e$) cross section or, at least, of the ν_μ/ν_e ($\bar{\nu}_\mu/\bar{\nu}_e$) ratio. A CC ν_e and $\bar{\nu}_e$ event selection was implemented. The selection efficiency of

CC-ν_e with an electron detected in one of the TPCs is shown in Fig. 34. The upgraded ND280 is able to detect many more electrons produced at high angles with respect to the neutrino direction. Electrons produced in the forward direction are less efficiently selected: the electron produces a shower inside the target and tend to stop after about 1 m. For this reason it becomes more important to detect electrons using the full information provided by the SD detector. It is clear that thanks to a good performance of the target detector, the total number of selected CC-ν_e events as well can be drastically improved.

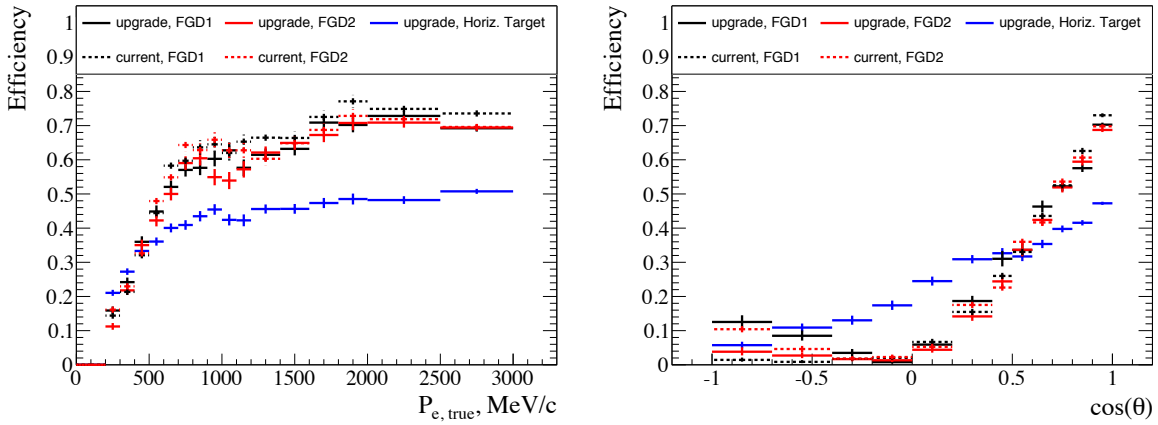

Figure 34: The ν_e selection efficiency, with an electron detected in a TPC, as a function of the electron angle is shown for both upgraded (solid lines) and current (dashed lines) ND280 configurations. The curves for FGD1 (black), FGD2 (red) and horizontal target (blue) are shown. The left plot shows the efficiency as a function of the electron momentum, while the right plot shows the efficiency as a function of the electron angle with respect to the Z direction.

10.3 Sensitivity studies

Sensitivity studies were performed to obtain quantitative informations on the impact of an upgrade of ND280 onto the oscillation analysis of T2K. The goals of the study were the following:

- evaluate how much we can improve the constraints on the flux and cross-section models;
- estimate the power to discriminate between different cross-section models.

The tools developed for the official T2K oscillation analysis, including ν_μ and $\bar{\nu}_\mu$ candidate event samples, were adapted and used for the study. The Monte-Carlo (MC) simulations was reweighted with the efficiencies and purities described in Sec. 10.1 and 10.2. The near detector fitter maximizes a binned likelihood ratio as a function of the neutrino flux, cross section and detector systematic parameters, all constrained with a penalty term except those related to the neutrino CCQE and 2p2h cross-section. This fitter is functionally identical to the fitter used in T2K oscillation analysis.

A set of uncorrelated systematic parameters was used to describe the detector systematics as a function of the muon true angle and momentum, for both the ND280 current and upgrade configurations fits.

Table 8: Detector systematic uncertainties parametrized as a function of the muon true momentum and angle with respect to the Z direction.

Detector configuration	Momentum / $\cos\theta$	$0 < p < 0.5$ GeV/c	$p > 0.5$ GeV/c
FGD1, FGD2	$-1 < \cos\theta < -0.6$	20%	20%
	$-0.6 < \cos\theta < 0$	50%	60%
	$0 < \cos\theta < +0.6$	30%	50%
	$+0.6 < \cos\theta < +1$	9%	2.5%
SD	$-1 < \cos\theta < -0.6$	9%	2.5%
	$-0.6 < \cos\theta < 0$	9%	2.5%
	$0 < \cos\theta < +0.6$	9%	2.5%
	$+0.6 < \cos\theta < +1$	9%	2.5%

Since in the ND280 upgrade configuration the high angle region is mostly covered by TPCs, we expect the detector systematic uncertainties to be about 2.5% above 0.5 GeV/c, assuming the same performance of the vertical TPCs currently used in ND280. In the ND280 current configuration the high angle region is covered only by the ECAL detector, where the detector systematic uncertainties are larger than 30%. In Table 8 the detector systematic uncertainties used in the sensitivity studies are shown.

The impact of the different detectors on the neutrino flux and cross-section constraints is evaluated by performing a fit of the Asimov data set, the most probable data set, corresponding to the MC expectation. The simulated beam exposure correspond to 8×10^{21} POT, about a third of the expected total data collected at the end of T2K-II. The sensitivity was obtained for both the ND280 upgrade and current ND280 configurations and compared. The post-fit errors of some of the most significant systematic parameters are shown in Table 9. On average the error on the systematic parameters is reduced by about 30%.

Table 9: Sensitivity to some flux and cross-section parameters of interest for the current ND280 and the upgrade configuration.

Parameter	Current ND280 (%)	Upgrade ND280 (%)
SK flux normalisation ($0.6 < E_\nu < 0.7$ GeV)	3.1	2.4
MA_{QE} (GeV/c^2)	2.6	1.8
ν_μ 2p2h normalisation	9.5	5.9
2p2h shape on Carbon	15.6	9.4
MA_{RES} (GeV/c^2)	1.8	1.2
Final State Interaction (π absorption)	6.5	3.4

In Fig. 35 the main post-fit systematic errors are shown. The ND280 upgrade-like configuration can provide overall smaller systematic uncertainties to the neutrino oscillation measurement.

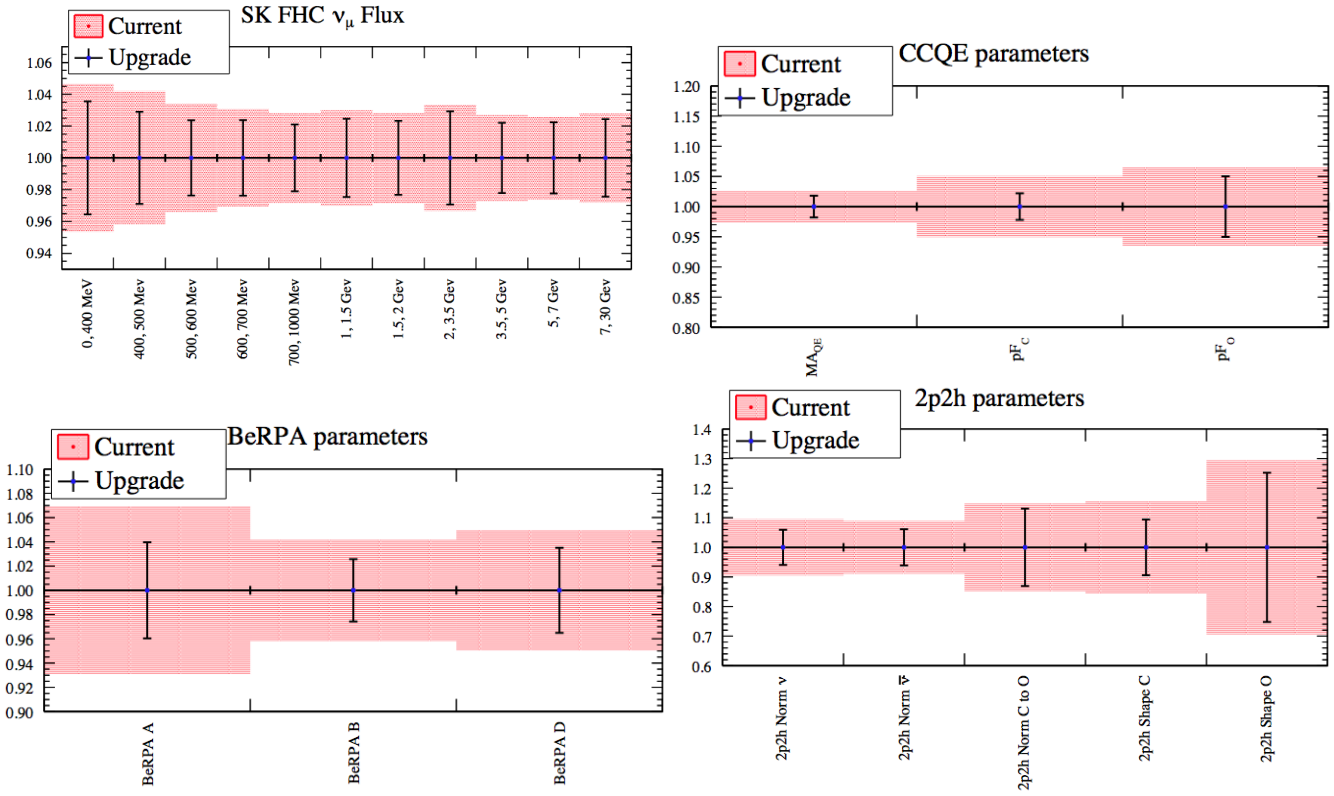

Figure 35: The post-fit errors on the main systematic parameters are shown for both the ND280 upgrade (blue dots) and the current ND280 configuration (red bars). These sets of parameters comprise the far detector ν_μ flux (top left), the CCQE cross-section (top right), the Random Phase Approximation (bottom left) and 2p2h parameters (bottom right).

The uncertainty on the total number of events selected at the T2K far detector, Super-Kamiokande (SK), was evaluated using the best-fit ND280 covariance matrix obtained by the Asimov data set fit. The neutrino cross-section parameters that cannot yet be constrained by the ND280 detector, like $\sigma_{\nu_e}/\sigma_{\nu_\mu}$ ratio and the NC parameters, are not propagated from ND280 to SK analysis. A comparison between the current ND280 and the upgrade configuration for different samples can be seen in Table 10. The uncertainty on the total number of events at SK is reduced by 20-30%. In this estimate potential constraints to the ND280-unconstrained systematic parameters, like $\sigma_{\nu_e}/\sigma_{\nu_\mu}$, are not included.

These studies provide an indication of the sensitivity of an upgraded detector configuration but are limited to a specific neutrino cross-section model. We know that the current model is not necessarily the correct and complete parametrization of the neutrino interactions for the full phase space. While this model is adequate for the current T2K analyses, which are still dominated by the statistical uncertainty, its shortcomings could be an issue when the systematic uncertainties will become as large as the statistical ones.

Table 10: Sensitivity to some flux and cross-section parameters of interest for the current ND280 and the upgrade configuration.

Source of uncertainty		ν_e CCQE-like $\delta N/N$ (%)	ν_μ $\delta N/N$ (%)	ν_e $CC1\pi^+$ $\delta N/N$ (%)
Flux + cross-section	Current ND280	2.22	2.27	2.08
(constrained by ND280)	Upgrade ND280	1.77	1.94	1.35

In order to provide useful informations on the importance of improving the ND280 angular acceptance, complementary studies were performed: assuming Nature behaves differently from the cross section model used for the neutrino events prediction, the bias on the neutrino flux and cross section systematic parameters was evaluated. A more sensitive detector configuration will provide larger biases in the best-fit parameters as well as a poorer goodness of fit (g.o.f.). Several alternative models were tested instead of the nominal prediction and it was found that, thanks to the largely improved angular acceptance and the increased target mass, the ND280 upgrade configuration was able to reject the alternative model with a better significance than the current ND280 configuration. In particular the models modifying the event distribution at high Q^2 showed a much worse g.o.f. and large biases.

We have performed these tests but their interpretation is still in progress. We plan to add these results and plots in 1-2 weeks.

11 Project organization

The group responsible for the ND280 upgrade works in the framework of the T2K collaboration. The group is strong of 218 physicists in 45 laboratories. It consists mainly of European and Japanese groups, with a developing participation of US institutes. Most of these groups were already active in the construction of the present ND280 detector. There are also specialists of MPGD and gas detectors in general, as well as of plastic scintillator detectors. It includes the proponents of the Super-FGD concept.

This group is structured in Work Packages presented in Table 11. It has been meeting regularly every two months both with open workshops and during the pre-meeting of the T2K collaboration meetings at JPARC, with bi-weekly phone meetings in between.

The participation of the various laboratories to the upgrade activities is summarized in Tables 12 and 13. According to this preliminary scheme, the full TOF detector will be provided by the University of Geneva.

The major milestones are shown in Table 14. A more detailed project GANTT chart is in preparation.

A separate Appendix reports the cost estimated for the deliverables as well as the contribution of each institute.

Table 11: Work Package structure.

WP	Task	Convener 1	Convener 2	Convener 3
0	ND280 Upgrade conveners	Marco Zito	Masashi Yokoyama (deputy)	
1	Mech. design and integ.	Marcela Batkiewicz	Thorsten Lux	Davide Sgalaberna
2	HA-TPC	Marco Zito		
3	SD	Masashi Yokoyama		
4	TOF	Yury Kudenko		
5	Test beam	Stefania Bordoni	Federico Sanchez	
6	High Pressure TPC R & D	Asher Kaboth	Morgan Wascko	
7	Simulation-Optimization	Davide Sgalaberna		
8	Physics Studies	Sara Bolognesi	Claudio Giganti	
9	DAQ	Giles Barr		
10	Software	Yoshi Uchida		

Table 12: Contributions by the institutes to the deliverables for the HA-TPC.

Deliverable	IFAE	INFN	LPNHE	Krakow	Saclay	Warsaw	CERN	RWTH
Field cage	X	X						
Micromegas				X	X	X	X	
Electronics			X		X	X		
Gas system							X	
Calibration						X		X

Table 13: Contributions by the institutes to the deliverables for the SD and TOF.

Deliverable	CERN	Geneva	INR	Japan	USA
Scintillator			X		X
Fibers				X	
MPPC				X	
Electronics	X	X		X	
Mechanics, assembly	X	X	X	X	
TOF		X			

Table 14: Major milestones.

Milestone	Date
Proposal	January 2018
Test beam for the TPC Prototype	October 2018
Test beam for the Super-FGD Prototype	October 2018
TDR	December 2018
Start Detector Construction	January 2019
Completion of the detector Construction	March 2021
Preparation for the Upgrade	June 2021
Installation in Japan	July -September 2021
Commissioning	October-December 2021

11.1 Proposed CERN contribution

We have identified several areas where CERN contribution will be very effective and help the project attain its objectives thanks to the CERN expertise and research infrastructure. These areas comprise

- The design and production of large area resistive Micromegas detectors in the EP/DT MPGD workshop (pending approval from the EP/DT department)
- the TPC gas system, for both the new HA-TPC and the existing TPCs. This deliverable will be based on the existing infrastructure at JPARC (gas shack, gas lines etc) and will take advantage of the standardized system using modular elements (mixer, flow-meters, purity monitors, etc.) and racks developed by EP/DT for a variety of gas detectors, including their PLC controlling units.
- specific test beam periods on the PS T9/T10 lines
- a support for the construction of the Super-FGD detector in particular its assembly, the mechanical structure and its front end electronics
- clean rooms for the integration of the TPCs and the Super-FGD, prior to their shipping to Japan.

These contributions have been defined through discussions with the CERN Neutrino Platform and the CERN Neutrino physics group.

References

[1] K. Abe et al. The T2K Experiment. *Nucl. Instrum. Meth.*, A659:106–135, 2011.

[2] K. Abe et al. Observation of Electron Neutrino Appearance in a Muon Neutrino Beam. *Phys. Rev. Lett.*, 112:061802, 2014.

[3] M. Hartz for the T2K Collaboration. T2K NEUTRINO OSCILLATION RESULTS WITH DATA UP TO 2017 SUMMER, 2017. https://kds.kek.jp/indico/event/25337/.

[4] KEK. KEK Project Implementation Plan, 2016. https://www.kek.jp/ja/About/OrganizationOverview/Assessment/Roadmap/KEK-PIP.pdf.

[5] K. Abe et al. Letter of Intent: The Hyper-Kamiokande Experiment — Detector Design and Physics Potential — . 2011.

[6] K. Abe et al. Physics potential of a long-baseline neutrino oscillation experiment using a J-PARC neutrino beam and Hyper-Kamiokande . *PTEP*, 2015:053C02, 2015.

[7] K. Abe et al. Hyper-Kamiokande Design Report, 2 2016. KEK Preprint 2016-21, ICRR-Report-701-2016-1.

[8] Ko Abe et al. Proposal for an Extended Run of T2K to 20×10^{21} POT . 2016.

[9] S. Bienstock et al. ND280 Upgrade Task Force report, 2016. T2K-TN-303 unpublished.

[10] ND280 Upgrade Open Workshops, 2017. https://indico.cern.ch/event/568177/ https://indico.cern.ch/event/613107/ https://indico.cern.ch/event/633840/ https://indico.cern.ch/event/644360/ https://indico.cern.ch/event/667631/ https://indico.cern.ch/event/673242/.

[11] P. Hamacher-Baumann et al. Near Detector based on gas TPCs for neutrino long baseline experiments, 2017. SPSC-EOI-015.

[12] K. Abe et al. Measurement of neutrino and antineutrino oscillations by the T2K experiment including a new additional sample of ν_e interactions at the far detector. *Phys. Rev. D*, 96:092006, 2017.

[13] N. Abgrall et al. Time Projection Chambers for the T2K Near Detectors. *Nucl. Instrum. Meth.*, A637:25–46, 2011.

[14] K. Abe et al. Measurement of the intrinsic electron neutrino component in the T2K neutrino beam with the ND280 detector. *Phys. Rev.*, D89:092003, 2014. [Phys. Rev.D89,099902(2014)].

[15] Ties Behnke, Klaus Dehmelt, Ralf Diener, Lea Hallermann, Takeshi Matsuda, Volker Prahl, and Peter Schade. A Lightweight Field Cage for a Large TPC Prototype for the ILC. *JINST*, 5:P10011, 2010.

[16] M. G. Catanesi et al. The HARP detector at the CERN PS. *Nucl. Instrum. Meth.*, A571:527–561, 2007.

[17] M. S. Dixit et al. Position sensing from charge dispersion in micro-pattern gas detectors with a resistive anode. *Nucl. Instrum. Meth.*, A518:721, 2004.

[18] Marie Di Marco et al. Test-bench for the characterization of MicroMegas modules for the T2K ND280 TPC. *J. of Phys. Conf. Series*, 65, 2007.

[19] Pascal Baron et al. Architecture and implementation of the front-end electronics of the time projection chambers in the T2K experiment. *IEEE Trans. Nucl. Sci.*, 57:406–411, 2010.

[20] Pascal Baron, Denis Calvet, Eric Delagnes, Xavier de la Broise, Alain Delbart, Frederic Druillole, Eduardo Monmarthe, Estelle Mazzucato, Francois Pierre, and Marco Zito. AFTER, an ASIC for the readout of the large T2K time projection chambers. *IEEE Trans. Nucl. Sci.*, 55:1744–1752, 2008.

[21] Shebli Anvar et al. AGET, the GET front-end ASIC, for the readout of the Time Projection Chambers used in nuclear physics experiments. *Proc. IEEE Nucl. Sci. Symp.*, pages 745–749, 2011.

[22] David Attie et al. The readout system for the Clas12 Micromegas vertex tracker. *Proc. 19th IEEE-NPSS Real Time Conference*, pages 1–11, 2010.

[23] C. Glattfelder. Mercury-ZX1 User Manual, 2015. Enclustra GmbH, 2015. www.enclustra.com.

[24] Davide Sgalaberna, A. Blondel, F. Cadoux, S. Fedotov, A. Korzenev, Y. Kudenko, A. Longhin, O. Mineev, E. Noah, and N. Yershov. A fully active fine grained detector with three readout views. 2017.

[25] Yu. G. Kudenko, L. S. Littenberg, V. A. Mayatsky, O. V. Mineev, and N. V. Ershov. Extruded plastic counters with WLS fiber readout. *Nucl. Instrum. Meth.*, A469:340–346, 2001.

[26] P. A. Amaudruz et al. The T2K Fine-Grained Detectors. *Nucl. Instrum. Meth.*, A696:1–31, 2012.

[27] Anna Pla-Dalmau. Extruded plastic scintillator for the MINOS calorimeters. *Frascati Phys. Ser.*, 21:513–522, 2001. [,513(2001)].

[28] Fuminao Hosomi et al. Performance test of new MPPC for a new neutrino detector WAGASCI. *PoS*, PhotoDet2015:046, 2016.

[29] M. Yokoyama et al. Performance of Multi-Pixel Photon Counters for the T2K near detectors. *Nucl. Instrum. Meth.*, A622:567–573, 2010.

[30] F. Moreau, J. C. Vanel, O. Drapier, M. Gonin, A. Bonnemaison, A. Cauchois, Y. Geerebaert, and S. Couturier-Le Quellec. Mass characterization of multi-pixel photon counters for the T2K 280-m near detector. *Nucl. Instrum. Meth.*, A613:46–53, 2010.

[31] A. Vacheret et al. Characterization and Simulation of the Response of Multi Pixel Photon Counters to Low Light Levels. *Nucl. Instrum. Meth.*, A656(1):69–83, 2011.

[32] Antonin Vacheret, Sarah Greenwood, Matt Noy, Mark Raymond, and Alfons Weber. The front end readout system for the T2K-ND280 detectors. In *Proceedings, 2007 IEEE Nuclear Science Symposium and Medical Imaging Conference (NSS/MIC 2007): Honolulu, Hawaii, October 28-November 3, 2007*, volume 3, pages 1984–1991, 2007.

[33] S. Conforti Di Lorenzo, S. Callier, J. Fleury, F. Dulucq, C. De la Taille, G. Martin Chassard, L. Raux, and N. Seguin-Moreau. SPIROC: Design and performances of a dedicated very front-end electronics for an ILC Analog Hadronic CALorimeter (AHCAL) prototype with SiPM read-out. *JINST*, 8:C01027, 2013.

[34] Etam Noah et al. Readout scheme for the Baby-MIND detector. *PoS*, PhotoDet2015:031, 2016.

[35] A. Blondel, D. Breton, A. Dubreuil, A. Khotyantsev, A. Korzenev, J. Maalmi, A. Mefodev, P. Mermod, and E. Noah. Study of timing characteristics of a 3 m long plastic scintillator counter using waveform digitizers. *Nucl. Instrum. Meth.*, A877:9–15, 2017.

[36] S. Gómez, D. Gascón, G. Fernández, A. Sanuy, J. Mauricio, R. Graciani, and D. Sanchez. MUSIC: An 8 channel readout ASIC for SiPM arrays. *Proc. SPIE 9899, Optical Sensing and Detection IV, 98990G*, 2016.

[37] C. Betancourt, A. Blondel, R. Brundler, A. Daetwyler, Y. Favre, D. Gascon, S. Gomez, A. Korzenev, P. Mermod, E. Noah, N. Serra, D. Sgalaberna, and B. Storaci. Application of large area SiPMs for the readout of a plastic scintillator based timing detector. *JINST*, 12:11023, 2017.

[38] C Andreopoulos et al. Proposal to Measure Hadron Scattering with a Gaseous High Pressure TPC for Neutrino Oscillation Measurements. Technical Report CERN-SPSC-2017-030. SPSC-P-355, CERN, Geneva, Sep 2017.

[39] S. Aoki et al. The T2K Side Muon Range Detector (SMRD). *Nucl. Instrum. Meth.*, A698:135–146, 2013.

[40] C. Andreopoulos et al. The GENIE Neutrino Monte Carlo Generator. *Nucl. Instrum. Meth.*, A614:87–104, 2010.

[41] J. Allison et al. Recent developments in Geant4. *Nucl. Instrum. Meth.*, A835:186–225, 2016.

[42] K. Abe et al. T2K neutrino flux prediction. *Phys. Rev. D*, 87:012001, 2013.